NEUROSCIENCE

Enhanced Rap1 small GTPase activity in the ventral hippocampus drives stress-induced anxiety

Han-Qing Pan[1]†, Wei-Zhu Liu[1,2]†, Cui-Zhu Yang[1]†, Si-Ying Jiang[1], Mao-Xue Zhang[1], Ping Hu[3], Hao-Tian Yang[1], Yun-Yun Wang[4], Ya-Qing Li[1], Jiang-Long Tu[1], Wen-Bing Chen[5], Lumin Liu[6], Bing-Xing Pan[1,7]*, Wen-Hua Zhang[1,2,7]*

Chronic stress exposure is a primary contributor to the development of anxiety disorders, closely associated with hippocampal dysfunction. However, the underlying molecular mechanism remains poorly understood. Here, using a mouse model of chronic restraint stress (CRS), we observed a notable increase in the activity, rather than its overall expression level, of hippocampal Rap1, a small guanosine triphosphatase belonging to the Ras superfamily. Pharmacological inhibition of Rap1 activity in the ventral hippocampus (vHPC) effectively mitigated CRS-induced anxiety. Cell type–specific manipulation of Rap1 activity revealed that Rap1 dysfunction in vHPC pyramidal neurons (PNs), but not in astrocytes or interneurons, contributed to CRS-induced anxiety-like behaviors. Mechanistically, the heightened Rap1 activity in vHPC PNs augmented their intrinsic excitability through Kv4.2 phosphorylation at the Thr^{607} site, which contributes to the onset of anxiety-like behaviors in mice following CRS. Overall, our study reveals a previously undescribed anxiogenic effect of Rap1 and highlights it as a potential target for therapeutic intervention in stress-related mental disorders.

INTRODUCTION

Anxiety disorder is one of the most common mental disorders worldwide and a major contributor to both the overall economic burden and personal suffering associated with these disorders (*1*, *2*). Although the current therapeutic strategies, such as psychotherapy and medication, are available to relieve anxiety-related symptoms, their overall effectiveness remains limited (*3*, *4*). A major challenge in advancing treatment lies in the incomplete understanding of the underlying pathogenesis of anxiety disorder, which has profoundly impeded the development of effective therapeutic agents. Thus, a thorough understanding of the factors affecting anxiety disorders and a detailed exploration of their pathological mechanisms are imperative for providing insights and guidance for relevant research and clinical practice.

The hippocampus has been implicated in regulating stress response and multiple psychiatric disorders including anxiety disorders (*5*, *6*). As can be structurally and functionally divided into dorsal and ventral parts, a plethora of studies has demonstrated that those distinct subregions are involved in diverse behavioral regulation (*7*). It is well established that the dorsal hippocampus (dHPC) is closely associated with learning and spatial memory, while the ventral hippocampus (vHPC) primarily influences emotional and motivated behaviors, including anxiety-like behaviors (*7*, *8*). This distinction is evidenced by the fact that excitotoxic or electrolytic lesions of the vHPC, but not the dHPC, result in an anxiolytic-like effect (*9*, *10*). Increasing evidence suggests that the dHPC also plays an essential role in regulating stress-induced anxiety (*11*, *12*), thereby indicating that the involvement and mechanisms of the hippocampus in chronic stress–induced anxiety disorders remain far from conclusive, necessitating further investigation.

The small G protein Rap1, a key member of the Ras superfamily, acts as a molecular switch by transitioning between its active form (Rap1-GTP) upon guanosine 5′-triphosphate (GTP) binding and inactive form (Rap1-GDP) after GTP hydrolysis, thereby regulating a plethora of cellular biological processes such as adhesion, polarity, differentiation, and growth (*13*–*17*). Within the central nervous system, Rap1 has garnered growing attention because of its extensive involvement in neural development, synaptic plasticity, and neuronal excitability, thus exerting a profound impact on learning and memory, as well as emotional expression (*18*–*25*). The disruption of the Rap1-related pathways has been implicated in the pathogenesis of various neuropsychological disorders, including schizophrenia and depression (*26*–*30*). A recent study reveals that Rap1 serves as a critical mediator responsible for stress-induced abnormalities in neuronal structure and function within the prefrontal cortex, thereby leading to cognitive dysfunction (*31*), indicating the notable involvement of Rap1 in stress-related deleterious effects. Nevertheless, little is known regarding its role in the development of chronic stress–induced anxiety and the underlying mechanisms.

To address these questions, we used an anxiety mouse model of chronic restraint stress (CRS) and unveiled a essential role of enhanced Rap1 activity in vHPC pyramidal neurons (vHPC PNs), but not interneurons (INs) or astrocytes, in the onset of anxiety-like behaviors induced by chronic stress. The anxiogenic effect of Rap1 activation is associated with the hyperexcitability of vHPC PNs through phosphorylation of the voltage-gated potassium channel Kv4.2 at the Thr^{607} site.

RESULTS

Chronic stress activates Rap1 in the mouse hippocampus

To determine the effect of chronic stress on Rap1 expression, we subjected the male C57BL/6J mice to CRS for 10 consecutive days

[1]Department of Neurology, The Second Affiliated Hospital, School of Basic Medical Sciences and Institute of Biomedical Innovation, Jiangxi Medical College, Nanchang University, Nanchang, China. [2]Department of Pathology and Jiangxi Institute of Respiratory Disease, The First Affiliated Hospital, Jiangxi Medical College, Nanchang University, Nanchang, China. [3]Institute of Translational Medicine, Nanchang University, Nanchang, China. [4]Laboratory of Cell Signal Transduction, School of Basic Medical Science, Henan University, Kaifeng, China. [5]School of Basic Medical Sciences, Guangzhou Medical University, Guangzhou, China. [6]Department of Sleep Medicine Center, LongHua Hospital Shanghai University of Traditional Chinese Medicine, Shanghai, China. [7]Jiangxi Province Key Laboratory of Brain Science and Brain Health, Jiangxi Medical College, Nanchang University, Nanchang, China.
*Corresponding author. Email: panbingxing@ncu.edu.cn (B.-X.P.); whzhang@ncu.edu.cn (W.-H.Z.).
†These authors contributed equally to this work.

(Fig. 1A), and then the anxiety-like behaviors of mice were evaluated using open field test (OFT) and the elevated plus maze test (EPMT). Compared to the unstressed control mice, the CRS-exposed mice spent far less time in the central area in the OFT and had fewer entries as well as reduced time to the open arms in the EPMT (Fig. 1, B to E). The total distance traveled remained unchanged in the OFT (Fig. 1, B and C), suggesting that CRS does not affect overall locomotor activity. These results verify that the CRS protocol can effectively induce anxiety-like behaviors.

Then, the hippocampi were dissected to assess the expression of Rap1 (Fig. 1, A and F). Somewhat unexpectedly, Western blot analysis showed that CRS had little effect on the total Rap1 protein levels (Fig. 1, G and H). As a small guanosine triphosphatase (GTPase), the active form of Rap1 serves as the primary functional state. To ascertain whether CRS affects Rap1 activation, we used a glutathione *S*-transferase (GST)-RalGDS fusion protein system, wherein RalGDS could specifically bind to the activated form of Rap1 (Rap1-GTP) (*32*). Then, the activated Rap1 could be pulled down using glutathione resin and detected by Western blotting (Fig. 1F; also see in Materials and Methods). We found that CRS induced a robust increase in the active form of Rap1 (Fig. 1, G and H), indicating that CRS activates Rap1 in the mouse hippocampus. To investigate whether the activation of Rap1 by CRS reflects a cumulative effect of repeated stress over 10 consecutive days or merely an acute response to the last episode of restraint stress, we subjected mice to single 2-hour acute restraint stress, followed by behavioral testing and assessment of Rap1 expression (fig. S1A). Consistent with previous findings, no significant differences in anxiety-like behaviors were observed between the control (Con) and acute restraint stress groups (*33*), indicating that a single episode of acute stress procedure does not induce persistent excessive anxiety (fig. S1, B to E). Moreover, no significant differences in total Rap1 or active Rap1 levels were detected between the two groups (fig. S1, F and G), suggesting that the increased Rap1 activity observed following CRS arises from the cumulative effects of repeated stress rather than being solely attributable to the last episode of restraint stress. To further test whether the increased Rap1 activity in the hippocampus also occurred in other stress paradigms, we then measured the activity of hippocampal Rap1 in mice experiencing chronic unpredictable stress (CUS) (fig. S2A). Similar to CRS, CUS significantly enhanced anxiety-like behaviors in mice (fig. S2, B to E) and also led to increased activated Rap1 but not total Rap1 (fig. S2, F and G). These findings suggest that the heightened Rap1 activity in the hippocampus may represent a shared molecular characteristic underlying diverse prolonged stress paradigms in mice.

Pharmacological inhibition of Rap1 activity in vHPC alleviates CRS-induced anxiety

We next sought to determine the effect of heightened Rap1 activity on the CRS-induced anxiety-like behaviors. Given that both dorsal and ventral parts of the hippocampus have been implicated in the regulation of anxiety (*9*–*12*), we bilaterally injected GGTI-298, a Rap1-specific inhibitor, into either the dHPC or vHPC of mice 30 min before daily restraint stress (Fig. 1, I and J, and fig. S3). Behavioral test results revealed that regardless of treatment with either vehicle or GGTI-298 in the dHPC, CRS mice exhibited notably decreased time in the central area of the OFT and reduced exploration in the open arms of the EPMT (Fig. 1, K to N), arguing against the involvement of dHPC Rap1 activity in regulating CRS-induced anxiety-like behaviors. By contrast, GGTI-298 treatment in vHPC effectively reversed the increased anxiety-like behaviors induced by CRS (Fig. 1, O to R). Collectively, these observations indicate an essential role of Rap1 activity, especially in the vHPC, in mediating the anxiogenic effect of CRS.

Rap1 activity in vHPC PNs modulates CRS-induced anxiety-like behaviors

Given that Rap1 has been implicated in PNs, GABAergic neurons, and astrocytes (*22*, *23*, *34*, *35*), a critical question then arises regarding the cell type–specific role of vHPC Rap1 in mediating chronic stress–induced anxiety-like behaviors. To answer this question, we first tested whether genetic deletion of Rap1 from different cell types in vHPC through adenoassociated virus (AAV) could rescue CRS-induced anxiety. AAVs carrying Cre recombinase with an enhanced green fluorescent protein (eGFP) (Cre-eGFP group), or only expressing eGFP reporter gene (eGFP-only group), under the control of *Gad67* (fig. S4, A and B), *GfaABC1D* (fig. S4, H and I), or *CaMKII*α promoters were bilaterally injected into the vHPC of $Rap1^{flx/flx}$ transgenic mice (Fig. 2, A and B). The efficiencies of the virus injection were confirmed by immunostaining assay (Fig. 2C and fig. S4, C and J). As shown in fig. S4, deletion of Rap1 in either INs or astrocytes did not manifest any discernible impact on CRS-induced increase in anxiety-like behaviors. Ablating Rap1 in PNs effectively alleviated the CRS-induced increase in anxiety-like responses (Fig. 2, D to G).

To provide direct evidence regarding the necessity of activated Rap1 in vHPC PNs for the manifestation of exaggerated anxiety-like behaviors caused by CRS, we constructed AAVs expressing a widely used dominant-negative mutant of Rap1 (T17N, hereafter referred to as Rap1-DN) fused with mCherry fluorescent protein under the control of the *CaMKII*α promoter (AAV-*CaMKII*α-Rap1-DN-2A-mCherry), thereby allowing us to specifically inhibit Rap1 activity in PNs (Rap1-DN-mCherry). The virus that only encodes mCherry (AAV-*CaMKII*α-2A-mCherry) was set as the mCherry group (Fig. 2H). Both AAVs were bilaterally injected into the vHPC (Fig. 2I). Three weeks later, we observed a significant decrease in the levels of active Rap1 in the Rap1-DN-mCherry group (Fig. 2J). Behaviorally, Rap1-DN expression profoundly prevented the CRS-induced increase in anxiety-like behaviors (Fig. 2, K to N), indicating that inhibiting Rap1 activity in vHPC PNs ameliorates the anxiogenic effects of CRS.

To determine whether increasing Rap1 activity is sufficient to induce anxiety-like behaviors in naive mice, we introduced another AAV strategy to specifically express constitutive active mutant of Rap1 (referred to as Rap1-CA) in vHPC PNs. AAV-*CaMKII*α-Rap1G12V-2A-mCherry (Rap1-CA-mCherry group) or AAV-*CaMKII*α-2A-mCherry (mCherry group) was bilaterally injected into the vHPC (Fig. 2O). Four weeks later, mCherry was found in the vHPC PNs, and active Rap1 was markedly increased in the Rap1-CA virus–injected mice, substantiating the effectiveness of the AAVs (Fig. 2, P and Q). Behavioral results showed that mice with overexpressed Rap1-CA-mCherry in vHPC PNs spent less time in the center area during the OFT and had less exploration of the open arms during the EPMT when compared to those mCherry virus–injected control mice (Fig. 2, R to U). Together, these findings indicate that the increased Rap1 activity in vHPC PNs is both necessary and sufficient for the effects of chronic stress on anxiety-like behaviors.

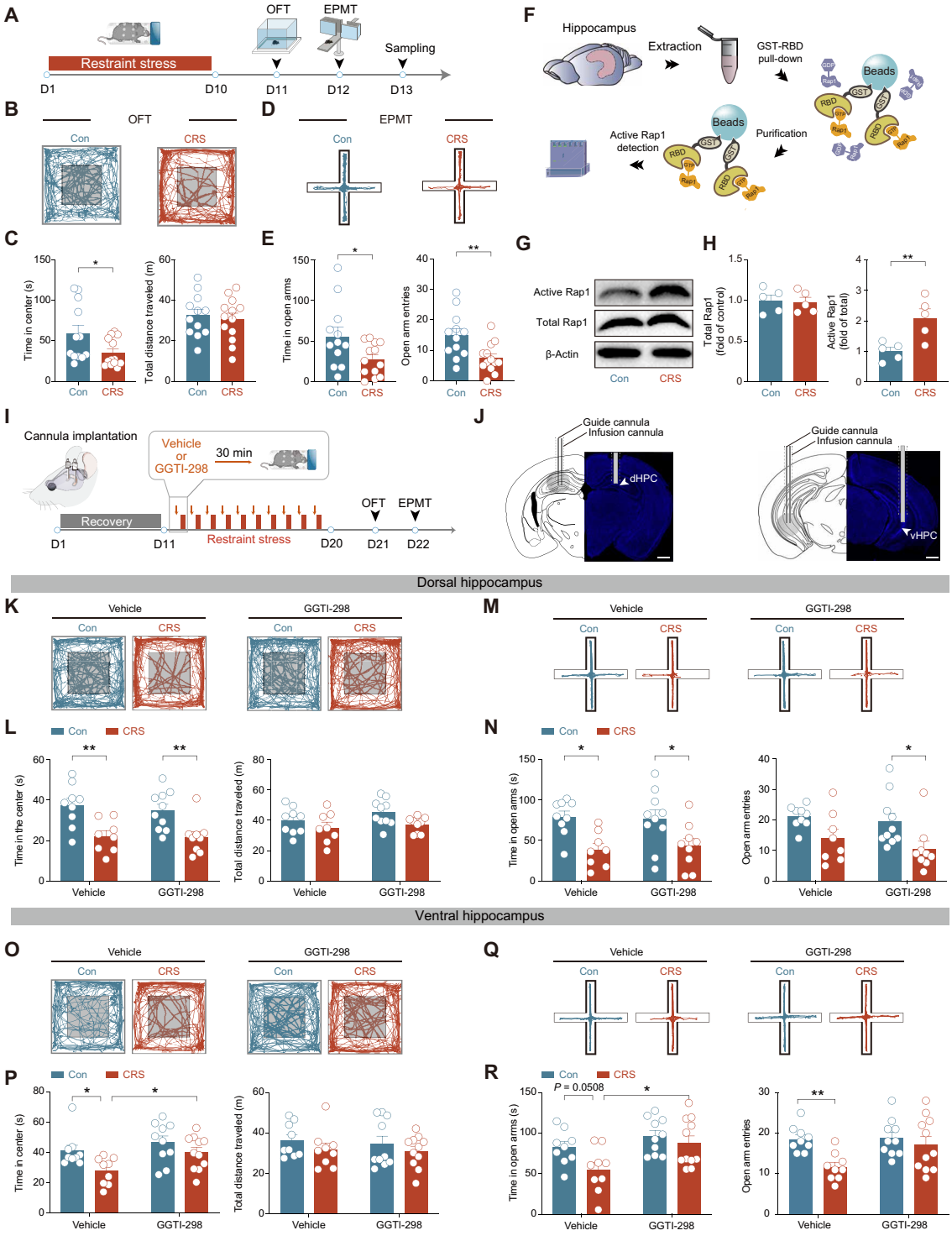

Fig. 1. Activation of Rap1 in the vHPC is essential for CRS-induced anxiety-like behaviors. (**A**) Experimental procedure for mice subjected to CRS. D, day. (**B** and **C**) Representative activity tracking and statistical analysis of time in the center and total distance traveled during OFT ($n = 12$ to 13 mice per group). (**D** and **E**) Representative activity tracking and statistical analysis of time in open arms and open arm entries during EPMT. Same sample size as in (C). (**F**) Scheme for the analysis of total Rap1 and active Rap1. (**G**) Representative Western blots from the Con and CRS mice. (**H**) Quantification analysis of relative total Rap1 and active Rap1 expression ($n = 5$ per group). (**I**) Scheme for delivering vehicle or GGTI-298 into the dHPC and vHPC. (**J**) Representative images of cannula implantation in dHPC and vHPC. (**K** and **L**) Representative activity tracking and statistical analysis of time in the center and total distance traveled during OFT of mice after administering vehicle and GGTI-298 in dHPC ($n = 8$ to 10 mice per group). (**M** and **N**) Representative activity tracking and statistical analysis of time in open arms and open arm entries during EPMT. Same sample size as in (L). (**O** to **R**) Same as in [(K) to (N)] except that the data were from mice receiving vehicle and GGTI-298 in vHPC ($n = 9$ to 11 mice per group). Data are presented as the means ± SEM. $^*P < 0.05$ and $^{**}P < 0.01$. Two-way ANOVA [(L), (N), (P), and (R)]; Mann-Whitney *U* test [(C), left]; two-tailed unpaired Student's *t* test [(C) right, (E), and (H)].

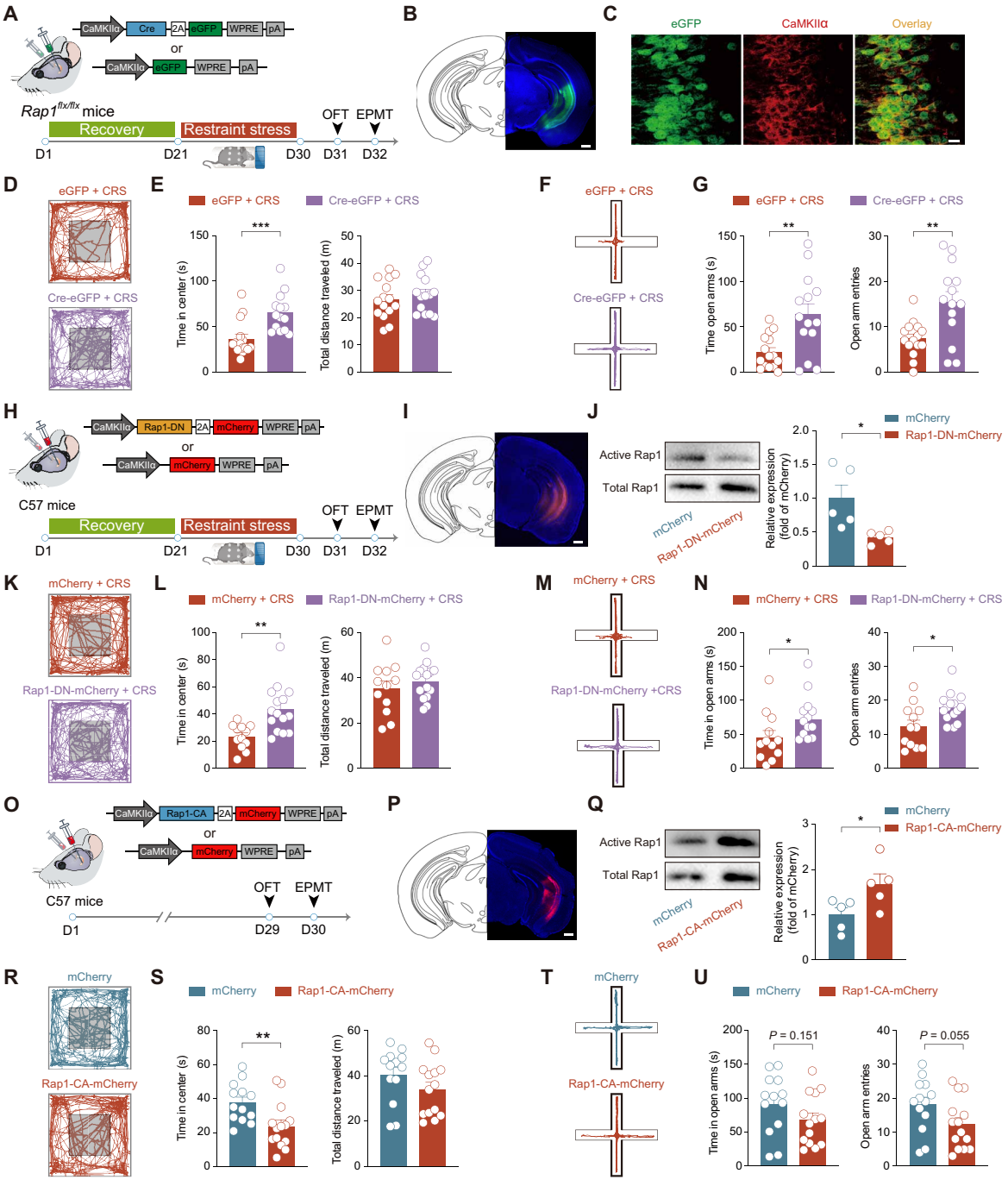

Fig. 2. Activation of Rap1 in vHPC PNs is required for CRS-induced anxiety-like behaviors. (**A**) Schematic of AAV injection to express Cre recombinase (Cre-eGFP) or eGFP alone (eGFP) under the *CaMKIIα* promoter in the vHPC of *Rap1*$^{flx/flx}$ mice followed by CRS and behavioral tests. (**B**) Representative images showing eGFP expression in vHPC. Scale bar, 500 μm. (**C**) Representative images of CaMKIIα immunostaining in the vCA1. Scale bar, 10 μm. (**D** and **E**) Representative activity tracking and quantification of time in the center and total distance traveled during OFT ($n = 14$ to 15 mice per group). (**F** and **G**) Representative activity tracking and quantification of time in open arms and open arm entries during EPMT. Same sample size as in [(D) and (E)]. (**H**) Schematic of overexpressing Rap1-DN-mCherry or mCherry alone in the vHPC PNs followed by CRS and behavioral tests. (**I**) Representative images showing mCherry expression in vHPC. Scale bar, 500 μm. (**J**) Representative immunoblots for active Rap1 and total Rap1 and statistical analysis of the immunoblotting assay from the mCherry and Rap1-DN-mCherry mice ($n = 5$ per group). (**K** to **N**) Same as in [(D) to (G)] except that the data were from mice infected with mCherry or Rap1-DN-mCherry ($n = 12$ to 15 mice per group). (**O**) Schematic of overexpressing Rap1-CA-mCherry or mCherry alone in the vHPC PNs and subsequent behavioral tests. (**P** and **Q**) Same as in [(I) and (J)] except that the data were from mice infected with mCherry or Rap1-CA-mCherry ($n = 5$ per group). (**R** to **U**) Same as in [(D) to (G)] except that the data were from mice infected with mCherry or Rap1-CA-mCherry and without subjecting to CRS ($n = 13$ to 14 mice per group). Pooled data are presented as the means ± SEM. $^*P < 0.05$, $^{**}P < 0.01$, and $^{***}P < 0.001$. Mann-Whitney *U* test [(E) left, (N) left, and (S) right]; two-tailed unpaired Student's *t* test [(E) right, (F), (J), (L), (N) right, (Q), (S) left, and (U)].

CRS or Rap1 activation elevates the neuronal activity of vHPC PNs

To determine how Rap1 activation in vHPC is involved in the anxiogenic effects mediated by CRS, we first assessed the impact of CRS and Rap1-CA overexpression on vHPC neuronal activity by using *c-Fos*, an immediate early gene for marking activated neurons (*36*). The mice were randomly assigned into three groups: mCherry, mCherry + CRS, and Rap1-CA-mCherry (Fig. 3A; also see in Materials and Methods). As shown in Fig. 3 (B and C), CRS remarkably increased the number of *c-Fos*–positive cells in ventral CA1 (vCA1) upon open arm exposure. This finding is consistent with previous study showing that chronic stress could notably increase the activation of vHPC neurons in response to acute stress stimuli (*37*). Moreover, the fluorescence intensity of *c-Fos*–positive cells was more prominent in both the mCherry + CRS and Rap1-CA-mCherry groups compared to the mCherry group (Fig. 3, D and E), indicating increased neuronal activity in the vHPC.

Considering the limitations of *c-Fos* immunostaining in detecting neuronal activity at a single time point, we further used in vivo fiber photometry to continuously monitor the real-time activity of vHPC PNs in freely moving mice. For this, the AAV encoding calcium indicator GCaMP6s was stereotaxically injected into vCA1 PNs, and an optic fiber was subsequently implanted over the vCA1 region that allowed us to observe Ca^{2+} transients during stressful conditions (i.e., exploring the EPM) (Fig. 3, F and G). Consistent with previous findings (*38*), we observed increased Ca^{2+} events in vHPC PNs when mice transitioned from the closed arms to the open arms of the EPM (Fig. 3, H and I). Such an increase was more pronounced in both the mCherry + CRS and Rap1-CA-mCherry mice compared to the mCherry ones (Fig. 3, H to J). Furthermore, we also observed Ca^{2+} transients in vHPC PNs when mice performed head dips, a highly anxiogenic behavior, at the edge of the open arms of the EPM (*38*, *39*). The CRS and Rap1-CA groups also exhibited a greater magnitude of Ca^{2+} transients (Fig. 3, K to M). Overall, these findings support the hypothesis that CRS enhances the neuronal activity of vHPC PNs, a phenomenon that can be mimicked by Rap1-CA overexpression in vHPC PNs.

Chemogenetic inhibition of vCA1 PNs alleviates Rap1 activation–induced anxiety

To investigate whether the hyperactivation of vHPC PNs, especially the vCA1 PNs, was responsible for CRS-induced anxiety, we attempted to acutely inhibit the activity of vCA1 PNs in CRS and Rap1-CA-mCherry mice before behavioral test. AAV-*CaMKII*α-hM4Di-GFP (Gi) was injected into the vHPC of CRS (fig. S5, A to C) and Rap1-CA (fig. S5, H and I) mice, allowing us to use clozapine-*N*-oxide, a biologically inert ligand, to inhibit the activity of hM4Di-expressing vCA1 PNs through the cannula. This localized delivery method allowed for precise modulation of neuronal activity in the targeted brain region (*40*). As shown in fig. S5, chemogenetically inhibiting vCA1 PN activity significantly alleviated anxiety-like behaviors in both CRS and Rap1-CA-mCherry mice. These results imply that the heightened activity of vCA1 PNs following CRS exposure or overexpression Rap1-CA is responsible for increased anxiety-like behaviors.

Rap1 activation spares the structure or synaptic transmission of vHPC PNs

It is well known that heightened neuronal activity may be attributed to the adaptive changes occurring in neurons themselves or through their communication with other interconnected cells. We subsequently asked whether chronic stress, through the activation of Rap1, reshapes the structure and synaptic transmission of vHPC PNs, thereby influencing their neuronal activity. To this end, we assessed the structure of vHPC PNs by performing whole-cell recordings on mCherry-positive cells with the biocytin-filled pipette (fig. S6A). Somewhat unexpectedly, we observed no statistically significant differences in dendritic complexity among the mCherry, mCherry + CRS, and Rap1-CA-mCherry groups (fig. S6, B and C). Analysis of dendritic spine density also revealed no significant differences in total dendritic spine density, as well as mature mushroom spine density, on both basal and apical dendrites among the three groups (fig. S6, D to G). In keeping with these findings, there were no significant differences in the amplitude and frequency of miniature excitatory postsynaptic currents (mEPSCs) in vHPC PNs (fig. S6, H and I). In addition, the amplitude and frequency of miniature inhibitory postsynaptic currents were also indistinguishable across these vHPC PNs (fig. S6, J and K). These findings suggest that chronic stress may not affect neuronal activity by altering the structure and synaptic transmission of vHPC PNs through the activation of Rap1.

Rap1 activation increases the intrinsic neuronal excitability of vHPC PNs

Aside from causing alterations in the neuronal structure and synaptic transmission, chronic stress has also been found to increase the activity of hippocampal neurons by modulating their intrinsic excitability (*41*–*44*). We then investigated the potential effects of CRS and Rap1 activation on the intrinsic excitability of vHPC PNs. Relative to the mCherry mice, the vHPC PNs from both mCherry + CRS and Rap1-CA-mCherry mice displayed more robust spike number upon the injection of depolarization current pulses (Fig. 4, A and B), indicating increased intrinsic neuronal excitability. Together with the *c-Fos* activation and increased Ca^{2+} activity following CRS or up-regulation of Rap1 activity, we hypothesized that increased Rap1 activity may be associated with the CRS-induced increase in the neuronal firing of vHPC PNs.

Next, we analyzed the shape of action potential (AP) to determine the potential mechanism by which CRS and up-regulation of Rap1 activity increased neuronal excitability. Analysis of the membrane properties of vHPC PNs showed that no significant differences were observed among the three groups in terms of their input resistance, resting membrane potential, AP threshold, and AP amplitude (fig. S7, A, B, and D to F). In addition, the sag ratio and medium and slow afterhyperpolarization potentials (AHPs), which have been implicated in influencing neuronal firing, did not differ across these three groups (fig. S7, A, B, and G to I). However, relative to the mCherry group, the fast AHP (fAHP) of neurons in mCherry + CRS and Rap1-CA-mCherry groups markedly decreased (Fig. 4, C and D), suggesting that the elevated intrinsic neuronal excitability in mCherry + CRS and Rap1-CA-mCherry mice may be attributed to the attenuation of fAHP.

Rap1 activation–induced hyperexcitability of vHPC PNs linked to I_A down-regulation

It is well established that fAHP is mainly mediated by the big-conductance calcium-activated potassium channel (BK channel) (*45*). To probe whether the BK channel was involved in CRS- and Rap1-CA–related inhibition of fAHP, we used tetraethylammonium (TEA), a selective BK channel blocker at low concentration (1 mM), to

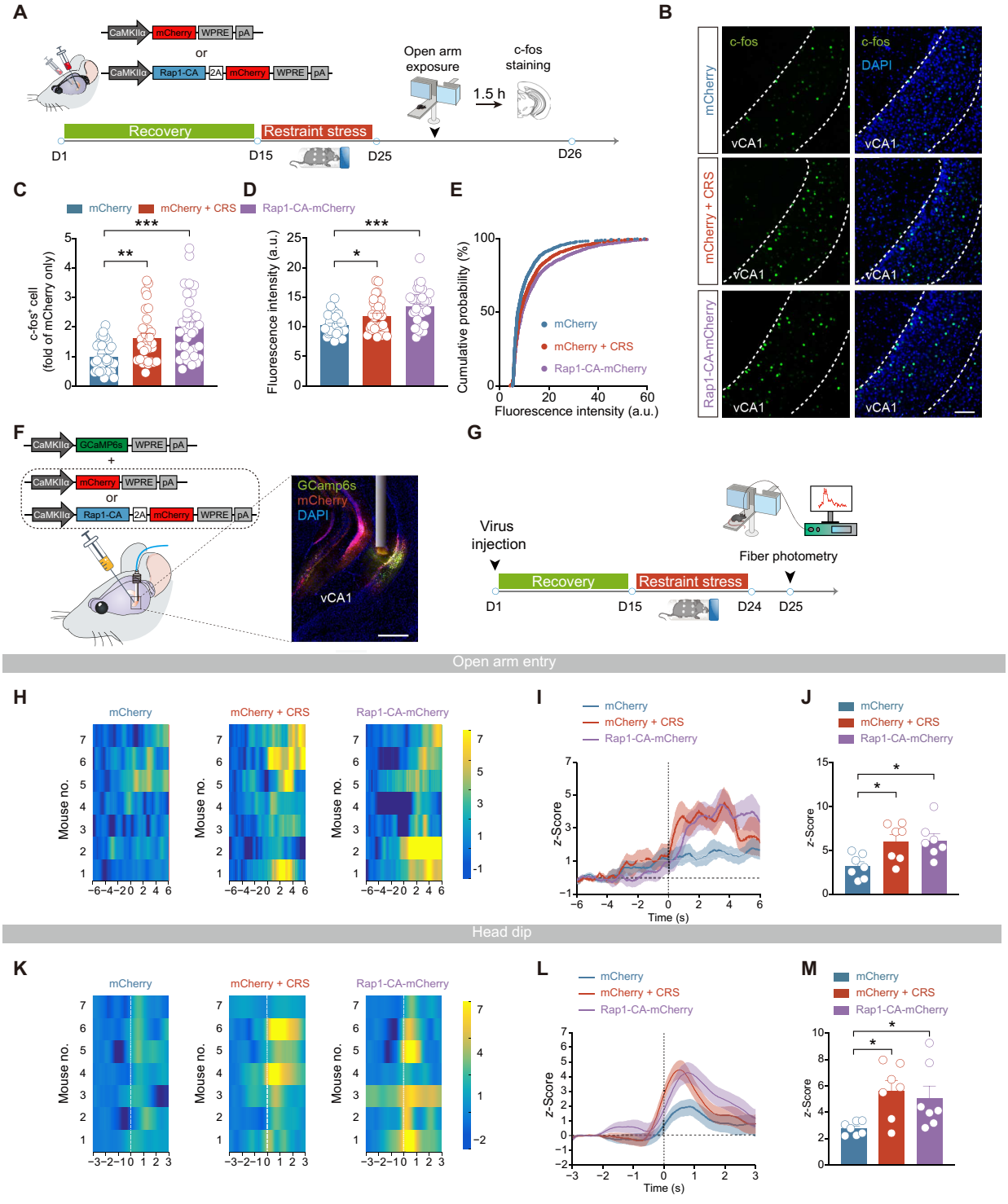

Fig. 3. CRS and Rap1 activation increase the neuronal activity of vCA1 PNs. (**A**) Schematics of virus injection, CRS procedure, and *c-Fos* immunostaining. h, hours. (**B**) Representative images of immunofluorescence showing *c-Fos* expression in the vCA1 in each group. Scale bar, 100 μm. (**C** and **D**) Quantification of the number and fluorescence intensity of *c-Fos*–positive cells in each group ($n = 31$ to 34 slices from four mice per group). a.u., arbitrary units. (**E**) Cumulative probability of c-Fos fluorescence intensity in vCA1 PNs. (**F**) Schematic depicting the virus injection strategy for recordings of the Ca^{2+} activity of vCA1 PNs and the representative image showing virus expression and optical fiber implantation site. Scale bar, 500 μm. (**G**) Experimental procedures for fiberphotometry recordings of Ca^{2+} activity. (**H** to **J**) Mean fluorescence, heatmap of fluorescence, and comparisons of Ca^{2+} transients of mice during entry into the open arms in EPM. $n = 7$ mice in each group. (**K** to **M**) Same as in [(H) to (J)] except that the signals are collected around head dips outside the edges of open arms. Data are presented as the means ± SEM. $^*P < 0.05$, $^{**}P < 0.01$, and $^{***}P < 0.001$. Kruskal-Wallis test [(C) and (D)]; one-way ANOVA [(J) and (M)].

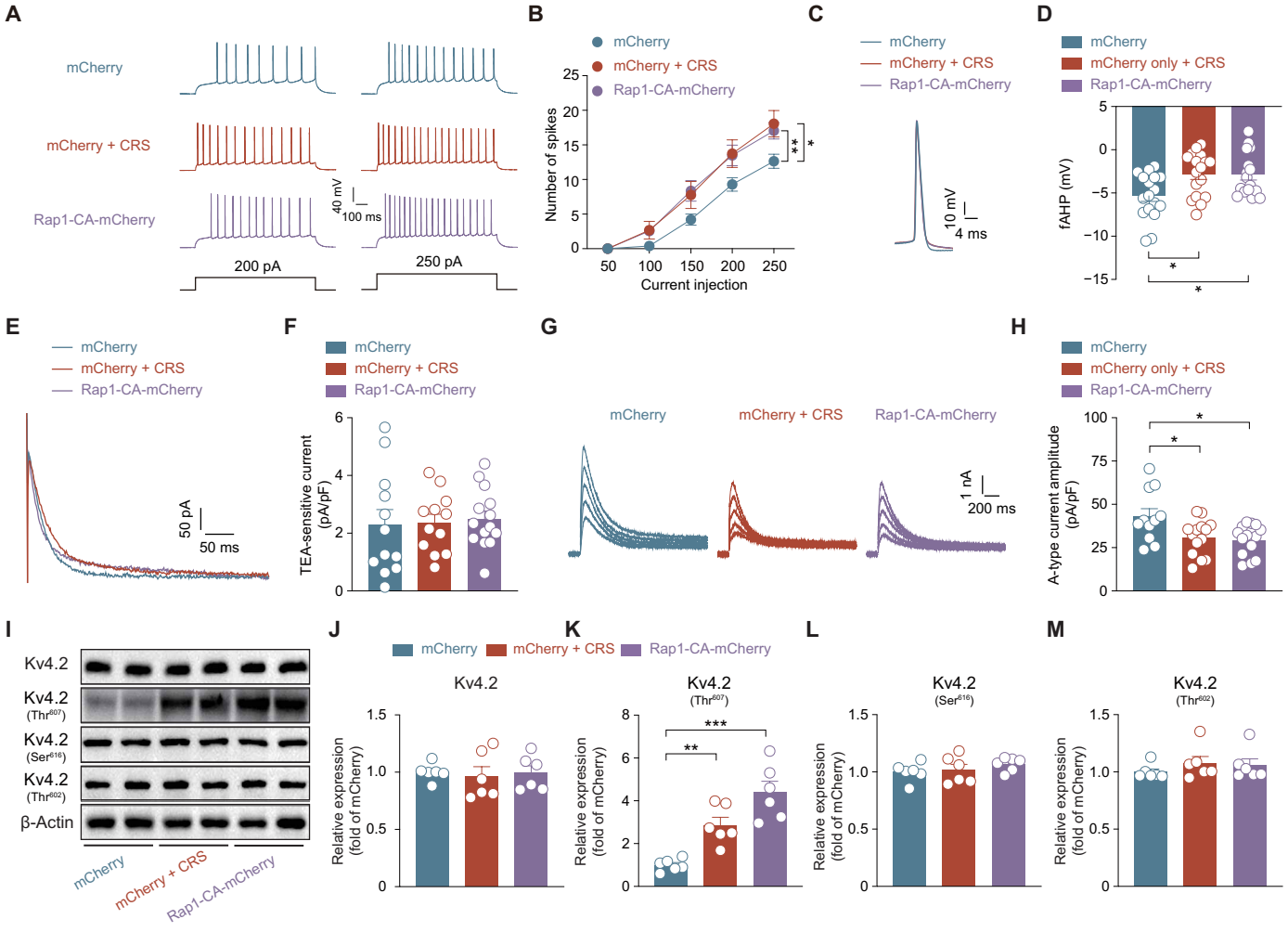

Fig. 4. CRS and Rap1 activation increase the intrinsic excitability of vHPC PNs. (**A**) Representative firing traces of vCA1 PNs in response to 200- and 250-pA depolarizing current injections. (**B**) Statistical analysis of AP numbers evoked by different depolarizing current injections ($n = 16$ to 17 neurons from five mice per group). (**C**) Representative fAHP traces. (**D**) Statistical analysis of fAHPs. Same sample size as in (B). (**E**) Representative traces showing TEA-sensitive big-conductance, calcium-activated potassium channel currents in vCA1 PNs. (**F**) Statistical analysis of TEA-sensitive currents ($n = 12$ to 14 neurons from five to six mice per group). (**G**) Representative traces showing transient A-type K^+ currents obtained at various voltages in vCA1 PNs. (**H**) Statistical analysis of transient A-type K^+ current densities recorded at +40 mV ($n = 11$ to 14 neurons from five to six mice per group). (**I**) Representative blots of the total Kv4.2, Kv4.2 Thr^{602}, Kv4.2 Thr^{607}, and Kv4.2 Ser^{616} in each group of mice. (**J** to **M**) Statistical analysis of total Kv4.2 (J), Kv4.2 Thr^{607} (K), Kv4.2 Ser^{616} (L), and Kv4.2 Thr^{602} (M) expressions ($n = 6$ mice in each group). Data are presented as the means ± SEM. $^*P < 0.05$, $^{**}P < 0.01$, and $^{***}P < 0.001$. Two-way ANOVA with repeated measures (B); Kruskal-Wallis test (M); one-way ANOVA [(D), (F), (H), and (J) to (L)].

isolate the BK channel–mediated current (I_{BK}) (*45*, *46*). Nevertheless, no significant differences were observed in TEA-sensitive current among the three groups of vHPC PNs (Fig. 4, E and F, and fig. S8, A and B), arguing against the involvement of the BK channel in this process. In addition to I_{BK}, A-type potassium current (I_A) has also been shown to be a notable contributor to the regulation of fAHP amplitude (*47*, *48*). By comparing the levels of I_A in the three groups of mice, we observed lower levels of I_A in both mCherry + CRS and Rap1-CA-mCherry groups compared to the mCherry group (Fig. 4, G and H, and fig. S8, C and D).

Rap1 activation increases Kv4.2 phosphorylation at the Thr^{607} site

Next, we explored how CRS and Rap1 activation affect I_A at the molecular level. I_A is mediated by a series of voltage-gated potassium channels (*49*); among them, Kv4.2 has the highest expression in the CA1 region of the hippocampus (*50*). To determine whether the changes in the functional activity of Kv4.2 contribute to the altered I_A in vHPC PNs, we assessed the total protein level of Kv4.2 in vHPC from mCherry, mCherry + CRS, and Rap1-CA-mCherry mice. However, no significant differences were observed in the total protein level of Kv4.2 among the three groups (Fig. 4, I and J). We then measured the phosphorylation levels of Kv4.2 at three specific sites: Thr^{602}, Thr^{607}, and Ser^{616}, known to be responsible for the I_A regulation (*47*, *51*, *52*). The phosphorylation level of the Thr^{607} site in Kv4.2 was significantly increased in both the mCherry + CRS and Rap1-CA-mCherry groups while leaving the phosphorylation levels of the other two sites unaltered among the three groups (Fig. 4, I to M).

Inhibiting Rap1 activity reverses the CRS-induced hyperexcitability of vHPC PNs

Then, we asked whether inhibiting Rap1 activity could reverse CRS-induced alteration in electrophysiological and molecular properties

of vHPC PNs (Fig. 5A). As shown in Fig. 5 (B and C), the excitability of these neurons in the Rap1-DN-mCherry + CRS group was significantly reduced compared to that in the mCherry + CRS group. In line with this, the fAHP and the I_A in the Rap1-DN-mCherry + CRS group were markedly enhanced (Fig. 5, D to G). Moreover, the increased Kv4.2 Thr^{607} phosphorylation provoked by CRS was also declined in Rap1-DN-mCherry + CRS mice (Fig. 5, H to L). Together, these data suggest that the suppression of I_A, which is mediated by the elevated phosphorylation level of Kv4.2 Thr^{607}, may act as an important contributor to mediate the effects of CRS and Rap1 overactivation on the neuronal excitability of vHPC PNs.

Kv4.2 Thr^{607} phosphorylation drives Rap1 activation–induced hyperexcitability and anxiety-like behaviors

To determine whether the increased phosphorylation of Kv4.2 at Thr^{607} contributes to the decreased I_A and subsequent increased neuronal excitability following CRS or overexpression of active Rap1, we generated AAV viruses expressing a mutant Kv4.2 where the threonine at site 607 was substituted with alanine under the control of the *CaMKIIα* promoter (Kv4.2-T607A group) (Fig. 6A). Western blot results confirmed the efficiency of the virus on decreasing phosphorylation of Kv4.2 at Thr^{607}, and electrophysiological recordings underscored the contribution of Kv4.2-T607A to the gain of function in I_A (Fig. 6, B and C). We then assessed the impact of overexpression of Kv4.2-T607A on CRS-induced anxiety. As indicated in Fig. 6 (D to G), CRS-induced pronounced anxiety-like behaviors were effectively alleviated by Kv4.2-T607A infection. These results imply that the anxiogenic effects of CRS could be readily mitigated by abolishing Kv4.2 Thr^{607} phosphorylation. We next investigated whether overexpression of Kv4.2-T607A in the vHPC region could diminish CRS-induced neuronal hyperexcitability. As expected, overexpression of Kv4.2-T607A sharply attenuated the neuronal excitability of vHPC

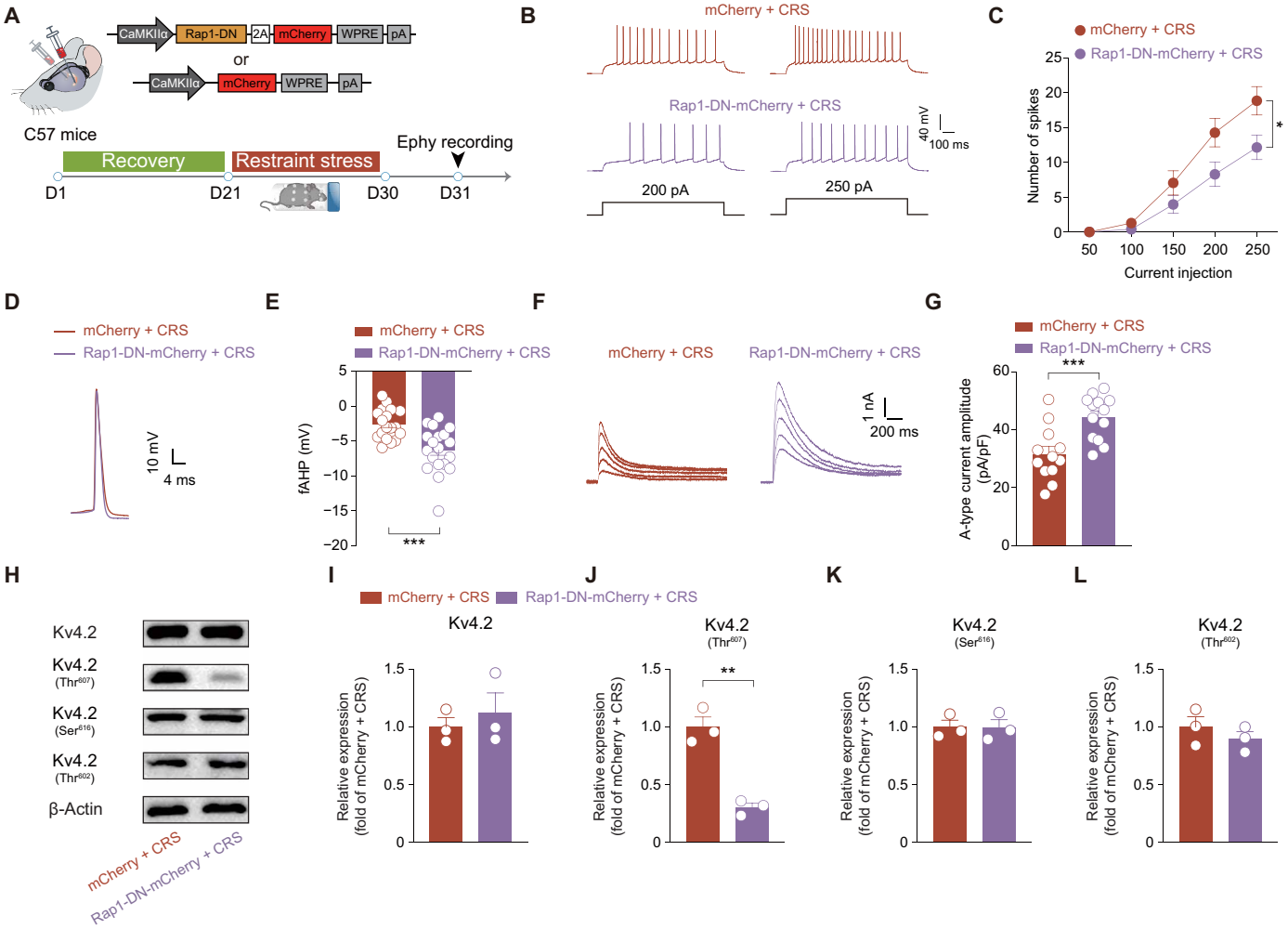

Fig. 5. Inhibiting Rap1 activity reverses CRS-induced hyperexcitability in vHPC PNs. (**A**) Schematics of AAV injections and subsequent CRS and electrophysiological experiments. (**B**) Representative firing traces of vCA1 PNs in response to 200- and 250-pA depolarizing current injections. (**C**) Statistical analysis of AP numbers evoked by different depolarizing current injections (n = 18 to 19 neurons from five mice per group). (**D**) Representative fAHP traces. (**E**) Statistical analysis of fAHPs. Same sample size as in (C). (**F**) Representative traces showing transient A-type K^+ currents obtained at various voltages in vCA1 PNs. (**G**) Statistical analysis of transient A-type K^+ current densities recorded at +40 mV (n = 12 to 13 neurons from six mice per group). (**H**) Representative blots of the total Kv4.2, Kv4.2 Thr^{602}, Kv4.2 Thr^{607}, and Kv4.2 Ser^{616} in mCherry + CRS and Rap1-DN-mCherry + CRS mice. Statistical analysis of total Kv4.2 (**I**), Kv4.2 Thr^{607} (**J**), Kv4.2 Ser^{616} (**K**), and Kv4.2 Thr^{602} (**L**) expressions in (H) (n = 3 mice in each group). Data are presented as the means ± SEM. *P < 0.05, **P < 0.01, and ***p < 0.001. Two-way ANOVA with repeated measures (B); two-tailed unpaired Student's t test [(E), (G), and (I) to (L)].

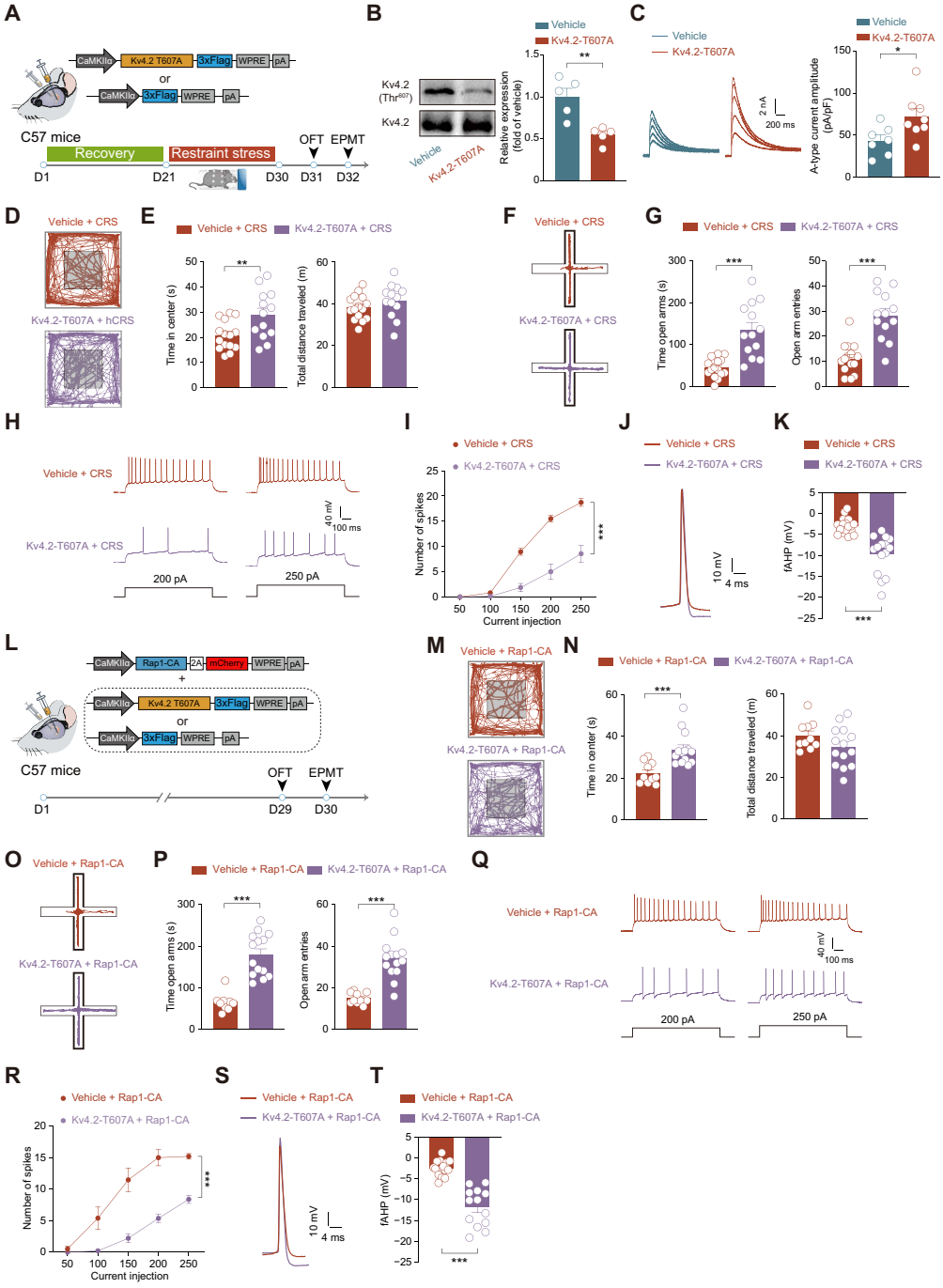

Fig. 6. Kv4.2 Thr^{607} phosphorylation drives Rap1 activation–induced anxiety-like behaviors and vCA1 PN hyperexcitability. (**A**) Experimental design for overexpressing Kv4.2-T607A (Kv4.2-T607A) or 3×FLAG alone (vehicle) in CRS mice and subsequent behavioral tests. (**B**) Representative blots and comparisons of the Kv4.2 Thr^{607} expression from vehicle and Kv4.2-T607A mice ($n = 3$ mice per group). (**C**) Representative traces showing transient A-type K^+ currents obtained at various voltages in vCA1 PNs and comparisons of transient A-type K^+ current densities recorded at +40 mV ($n = 7$ to 8 neurons from three mice per group). (**D**) Representative activity tracking in OFT. (**E**) Statistical analysis of time in the center and total distance traveled during OFT ($n = 13$ to 15 mice per group). (**F**) Representative activity tracking in EPMT. (**G**) Statistical analysis of time in open arms and open arm entries during EPMT. Same sample size as in (E). (**H**) Representative firing traces of vCA1 PNs in response to depolarizing current injection. (**I**) Statistical analysis of AP numbers evoked by different depolarizing current injections in (H) ($n = 15$ to 19 neurons from four to five mice per group). (**J**) Representative fAHP traces. (**K**) Statistical analysis of fAHPs in (J). Same sample size as in (I). (**L**) Schematic depicting the virus injection strategy for inhibiting phosphorylation of Kv4.2 at Thr^{607} in Rap1-CA mice and subsequent behavioral tests. (**M** to **T**) Same as in [(D) to (K)] except that the data were from vehicle + Rap1-CA and Kv4.2-T607A + Rap1-CA mice [(M) to (P), $n = 10$ to 14 mice per group; (Q) to (T), $n = 13$ to 15 neurons from four mice per group]. Data are presented as the means ± SEM. $^*P < 0.05$, $^{**}P < 0.01$, and $^{***}P < 0.001$. Two-way ANOVA with repeated measures [(I) and (R)]; Mann-Whitney *U* test [(N) left, and (P) left]; two-tailed unpaired Student's *t* test [(B), (C), (E), (G), (K), (N) right, (P) right, and (T)].

PNs following CRS (Fig. 6, H and I). Consistent with these results, CRS-induced suppression of fAHP was also reversed in Kv4.2-T607A mice (Fig. 6, J and K). To determine whether the heightened phosphorylation of Kv4.2 at Thr^{607} acts as a downstream effector of Rap1 activation, we bilaterally coinjected AAV-Rap1-CA with either AAV-*CaMKII*α-Kv4.2-T607A-3×FLAG (Kv4.2-T607A + Rap1-CA group) or AAV-*CaMKII*α-3×FLAG (vehicle + Rap1-CA group) into the vHPC (Fig. 6L). Subsequently, we assessed behavioral changes and neuronal excitability associated with Rap1-CA overexpression. As shown in Fig. 6 (M to T), overexpression of Kv4.2-T607A mitigated Rap1-CA–induced excessive anxiety-like behaviors and hyperexcitability of vCA1 PNs. Collectively, these findings underscore the excessive Kv4.2 phosphorylation at Thr^{607} as a critical downstream mediator in Rap1 activation–induced hyperexcitability of vHPC neurons and anxiety-like behaviors in mice following chronic stress exposure.

DISCUSSION

In this study, we present evidence highlighting the critical role of Rap1 activity in vHPC PNs in regulating neuronal excitability and anxiety-like behaviors induced by chronic stress (Fig. 7). Specifically, we observed a marked increase in anxiety levels and Rap1 activity, rather than total protein levels, within the hippocampus following chronic stress exposure. Deletion or inhibition of Rap1 activity in vHPC PNs effectively mitigated the anxiogenic effects of CRS, whereas enhancing Rap1 activity in these neurons exacerbated anxiety-like behaviors. Further mechanistic evidence indicates that the heightened Rap1 activity leads to the hyperexcitability of vHPC PNs, a process closely associated with the down-regulation of I_A through phosphorylation of Kv4.2 at the Thr^{607} site.

As a pivotal molecular switch, Rap1 plays an essential role in the regulation of multiple cellular processes. Recent studies have shown increased Rap1 expression in the synaptoneurosome of the mouse medial prefrontal cortex (mPFC) and dHPC following escalating, intermittent stress (*31*, *53*). In addition, pathway analysis revealed a significant down-regulation of the Rap1 signaling pathway in hippocampal astrocytes after parental isolation stress in postnatal day 7 mice (*54*). These findings suggest the involvement of Rap1 and its signaling pathways in stress-induced effects. However, our current study revealed that chronic stress did not affect the total Rap1 expression levels. By contrast, it did elicit a pronounced increase in Rap1 activity within the hippocampus following both CRS and CUS. To our knowledge, this represents the initial evidence indicating the participation of Rap1 activity in mediating the responses to chronic stress. We here observed a sustained elevation in Rap1 activity even 3 days after the last episode of a 10-day CRS protocol. In contrast, single acute restraint stress had no significant effect on the levels of total Rap1 or active Rap1. These findings suggest that the increased Rap1 activity induced by CRS arises from the cumulative outcome of repeated stress exposure rather than being a transient response to a single stress episode. This underscores the critical role of repeated stress in driving persistent molecular and neuronal changes linked to anxiety-like behaviors. However, the duration for which Rap1 activation persists following CRS remains unclear. Previous research has shown that 10-day chronic immobilization stress produces a prolonged anxiogenic effect, even after 21 days of stress-free recovery (*55*). Whether the elevated Rap1 activation can be sustained over such an extended period warrants further investigation. In addition, the mechanism by which chronic stress activates Rap1 still remains an open question. Noteworthily, Rap1's activity is finely tuned by Rap1 guanine nucleotide exchange factors (GEFs) and Rap1 GTPase–activating proteins (GAPs), which balance its active and inactive states. GEFs activate Rap1 by facilitating the exchange of GDP for GTP, while GAPs enhance GTP hydrolysis, thereby resulting in the inhibition of Rap1 activity (*17*). One possible explanation for the persistent activation of Rap1 observed in our study may be linked to the disruption of the balance between Rap1GEFs and Rap1GAPs activities following chronic stress exposure. Further investigations are imperative to unveil the exact molecular mechanisms underlying this phenomenon.

Next, we provide compelling evidence demonstrating the increased Rap1 activity in vHPC PNs as a critical factor in the regulation of chronic stress–induced anxiety. First, pharmacological

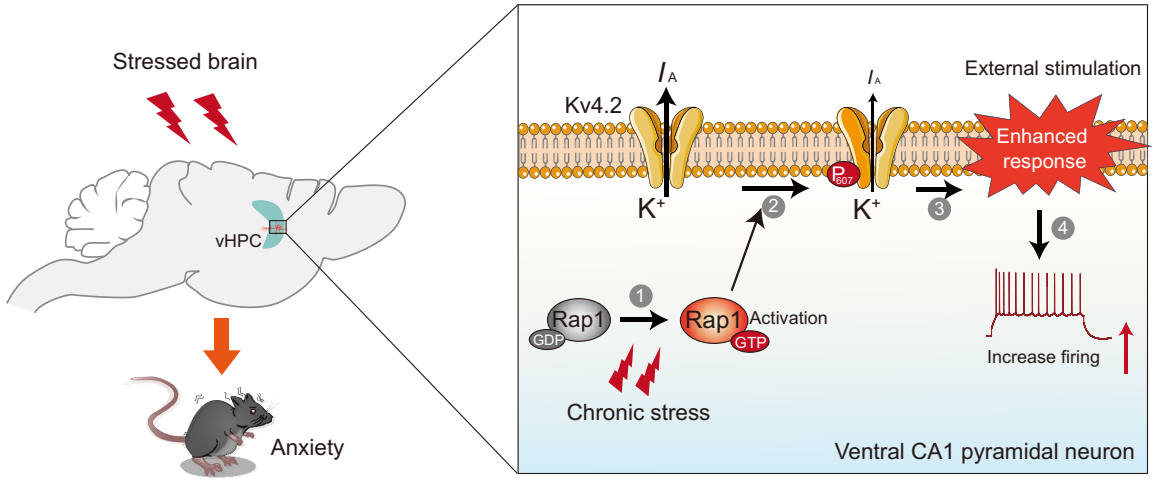

Fig. 7. Working model for Rap1 in mediating chronic stress–induced anxiety. Chronic stress triggers prolonged Rap1 activation in vHPC PNs, facilitating the phosphorylation of Kv4.2 at Thr^{607} and diminishing its channel activity. Consequently, when exposed to external anxiogenic environmental cues, the responsiveness of these neurons is heightened, leading to an anxiogenic effect.

inhibition of vHPC Rap1 activation during CRS effectively reduced the anxiety-like behaviors in mice. Second, selective deletion of Rap1 or overexpression of a dominant-negative Rap1 mutant (Rap1-DN) in vHPC PN suppressed the anxiogenic effects induced by CRS. Last, overexpression of a constitutively active Rap1 mutant (Rap1-CA) in the vHPC PN of unstressed mice was sufficient to increase anxiety-like behaviors. Intriguingly, inhibiting dHPC Rap1 activity or knocking out Rap1 in vHPC astrocytes or INs had a minimal effect on anxiety-like behaviors. It is noteworthy that the potential involvement of Rap1 activity in this specific subregion or cell type cannot be disregarded with respect to the regulation of other stress-related behaviors. Notably, a recent study by Bjornson *et al.* (*53*) has demonstrated that the overexpression of Rap1 in the dorsal CA3 region impairs cognitive behavior in mice, suggesting that the increased expression/activity of Rap1 may be implicated in distinct pathological effects of chronic stress, specifically in a subregion- and cell type–dependent manner.

Rap1 has been shown to regulate the neuronal structure and excitatory synaptic transmission, consequently leading to behavioral modifications. For instance, in cultured hippocampal neurons, inhibiting Rap1 activity by overexpressing Rap1-DN causes dendritic hypertrophy (*56*) and increased α-amino-3-hydroxy-5-methyl-4-isoxazole-propionicacid receptor–mediated currents (*18*, *57*). Conversely, overexpressing Rap1-CA to increase Rap1 activity decreases the amplitude and frequency of mEPSCs (*56*). In the mPFC, excessive Rap1 activation results in spine loss in PNs and cognitive impairment (*31*). However, we here failed to observe significant effects of Rap1 activation on dendritic branching, spine density, or the amplitude and frequency of mEPSCs in vHPC neurons, suggesting that the chronic stress–induced Rap1 overactivation in vHPC PNs on anxiety is unlikely tied to its ability to modify the neuronal structure and synaptic transmission. In considering this inconsistency, one potential interpretation is that Rap1 may act differently under varying conditions (cultured neurons versus brain tissue) and distinct brain regions (mPFC versus vHPC). Notably, the integrity of the neuronal structure and synaptic transmission also remained unchanged following CRS exposure, and Rap1 activation induced by CRS may not account for the heightened anxiety-like behaviors through modulation of the neuronal structure and synaptic transmission.

Instead, we propose that the heightened intrinsic excitability of vHPC PNs is the underlying cause for the augmented anxiety-like behaviors induced by CRS and Rap1 overactivation. As a key region within the limbic system, vHPC is closely associated with the regulation of anxiety-like behaviors under both physiological and pathological conditions. Specifically, it has been shown that the Ca^{2+} activity of vHPC PNs significantly increases during exploration of the open arms of EPMT, and this activity positively correlates with anxiety levels of individuals (*38*). While lesioning or optogenetic inhibition of vHPC PNs yields a conspicuous reduction in anxiety (*9*, *38*, *58*), chemogenetic activation of vHPC neurons engenders a remarkable augmentation in anxiety-like behaviors (*59*). In the present study, we observed that accompanied by their heightened anxiety levels, the neuronal activity and excitability were substantially increased within the vCA1 region in both CRS- and Rap1-CA–overexpressing mice. Together with the evidence that chemogenetic inhibition of vHPC PNs in these two groups successfully mitigated their anxiety-like behaviors, our findings highlight that changes in the intrinsic excitability of vCA1 PNs play a crucial role in mediating anxiety through Rap1 activation. In keeping with our findings, the activity and intrinsic excitability of vHPC PNs are significantly increased in the mouse model with conditions linked to heightened anxiety, such as CUL3-deficient mice (*60*) or mice with neuralgia-induced anxiety (*61*). Notably, there is also study indicating that chronic social defeat stress has a minimal effect on the intrinsic excitability of vCA1 PNs (*42*). This discrepancy may be attributed to the substantial heterogeneity of vCA1 PNs, which may exhibit different responses to various stressors.

Another important finding in the current study was the demonstration of the down-regulation of I_A, which is mediated by Kv4.2 as a physiological mechanism underpinning the heightened intrinsic excitability. Intriguingly, such down-regulation does not arise from the change in the total Kv4.2 expression but rather from increased Kv4.2 phosphorylation at the Thr^{607} site, which is consistent with previous studies showing that phosphorylation of Kv4.2 modulates I_A amplitudes and neuronal excitability (*47*, *51*, *62*). The question of such specificity remains open. Of note, Rap1 has been shown to activate various downstream effectors, including MEK, p38, B-Raf-MEK-ERK, PI3K-Akt, and AF6 (*17*). Among these, ERK and p38 kinases are known to regulate Kv4.2 phosphorylation and subsequent neuronal excitability (*22*, *47*, *51*, *63*). In particular, the p38 kinase exhibits a preference for phosphorylating the Thr^{607} site of Kv4.2 in response to stressors like novel environments or seizures (*47*, *62*). It would be interesting to determine whether p38 serves as the potential mediator of Kv4.2 Thr^{607} phosphorylation following Rap1 activation.

In addition to our findings, adaptive changes in the expression and function of Kv4.2 have also been observed in various brain regions in response to stress (*52*, *64*). For example, a 3-week CUMS protocol increased Kv4.2 Ser^{616} phosphorylation in the NAc, leading to a decrease in I_A levels (*52*). Moreover, a 10-day chronic social defeat stress or three-week CRS regimen reduced the expression of Kv4.2 in the lateral hypothalamic area GABAergic neurons, resulting in heightened neuronal excitability (*64*). These studies, together with our findings, highlight the pivotal role of Kv4.2 dysfunction as a critical mediator in the pathogenesis of stress-related behaviors and underscore the potential clinical translation value of pharmacologically enhancing Kv4.2 function. However, to the best of our knowledge, no pharmacological agents have been developed that act as Kv4.2 openers. Considering the crucial role of Kv4.2 in stress-related psychopathology, the development of Kv4.2-targeted therapeutics represents a promising and important direction for future research. Notably, recent advancements in cryo–electron microscopy have provided detailed structural insights into Kv4.2 (*65*–*68*), which will be instrumental in guiding the rational design and development of specific drugs targeting Kv4.2. Such efforts hold substantial potential for creation of therapeutic strategies to address stress-induced mental disorders.

Together, our findings shed light on a previous unrecognized role of the small G protein Rap1 in regulating CRS-induced anxiety through modulation of intrinsic excitability in vHPC. Nevertheless, it remains to be determined what molecular mechanisms are involved in the up-regulation of Rap1 activity by chronic stress. Second, vHPC PNs with different neuronal projections and molecular profiles exhibit distinct and even opposing roles in different behavioral tasks (*69*). For instance, activation of the mPFC and hypothalamus-targeting vHPC PNs increases anxiety-like behaviors in mice (*38*, *70*). While activation of Calb1-positive vHPC PNs displays anxiolytic effects, activation of Calb1-negative ones exhibits anxiogenic effects (*71*, *72*). Therefore,

comprehending how heightened Rap1 activity in vHPC PNs, which are integrated into distinct circuits with diverse behavioral outcomes, fine tunes vHPC-related behaviors such as anxiety regulation and fear memory encoding holds promise for future investigations.

MATERIALS AND METHODS

Animals

C57BL/6J (stock no. N000013, GemPharmatech, China) and *Rap1*$^{flx/flx}$ (stock no. 021066, the Jackson Laboratory, US) mice were used in this study. The detailed information of *Rap1*$^{flx/flx}$ mice was described previously (*21*). Two to five mice were raised in standard mice cages under the condition of a 12-hour light/dark cycle (light on at 07:00 a.m.) in a constant ambient temperature (24 ± 1°C) with ad libitum access to food and water. All experimental procedures were approved by the Animal Care and Use Committee of Nanchang University.

Chronic restraint stress

Mice were randomly divided into a stressed group and a nonstressed group. The stressed group of mice was subjected to a restraint cylinder closely fitted to their body size for 2 hours per day at 10:00 a.m. for 10 consecutive days. The nonstressed control mice were transferred to the experimental room from their home cages and gently handled for 5 min before being returned to the holding room 2 hours later.

Chronic unpredictable stress

Mice were subjected to a variety of stressors at different times of the day for 10 consecutive days. The stressors included the following: 2-hour restraint, 15-min tail suspension, 24-hour constant light exposure, 24-hour wet bedding with a 45° cage tilt, 2-hour rotation, 10-min inescapable foot shocks, and 8-min forced swim in 18°C water, 2-hour cold stress at 4°C, overcrowding overnight, and 20-min trimethylthiazoline exposure. All stress exposure was conducted in a procedure room.

Elevated plus maze test

Animals were habituated to the testing room for 30 min before experimentation and then rapidly placed into the central platform facing an open arm of a plus-shaped maze composed of two closed arms and two open arms. During the behavioral test, a video-tracking system was used to monitor their behavior for 10 min. The maze was cleaned with 75% ethanol between each trial. The time spent in open arms and entries into the open arms were analyzed using ANY-maze software (Stoelting Co., US).

Open field test

After being habituated to the testing room for 30 min, each mouse was gently placed in the center of a field apparatus (50 by 50 cm) and allowed to explore the arena for 10 min, monitored by an overhead video-tracking system. The field apparatus was cleaned with 75% ethanol between each trial. The time mice spent in the center area and the total distance they traveled during each test were analyzed using ANY-maze software.

Stereotaxic surgery

The stereotaxic surgery was performed as described previously (*73*). Briefly, 4-week-old male mice were anesthetized with an intraperitoneal injection of 2% pentobarbital sodium and placed in a stereotaxic frame (RWD Life Science Co., Ltd., China). For AAV injection, a specific volume of the virus was bilaterally injected into the vHPC (posterior to bregma, AP = −3.42 mm; lateral to the midline, ML = ±3.42 mm; below the bregma, DV = −3.95 mm) or dHPC (AP = −1.90 mm; ML = ±1.85 mm; DV = −1.40 mm) with a glass micropipette using a stereotactic injector (RWD Life Science Co., Ltd., China). For cannula implantation, the guide cannula (RWD Life Science Co., Ltd., China), together with an infusion cannula, was bilaterally implanted into the dHPC and vHPC with the same coordination site as virus injection or vCA1 (AP = −3.42 mm; ML = ±3.55 mm; DV = −3.80 mm), respectively.

Histology and microscopy

Anesthetized mice were transcardially perfused with 0.9% saline followed by 4% paraformaldehyde (PFA) in 0.1 M phosphate-buffered saline (PBS). Brains were postfixed overnight at 4°C in 4% PFA. Then, 40-μm-thick slices containing the dHPC or vHPC were cut using the VT1200S Vibratome (Leica Microsystems, Wetzlar, Germany). The slices containing the dHPC or vHPC were washed three times in PBS for 5 min. Sections were then blocked in permeable buffer containing 10% normal donkey serum and 0.1% Triton X-100 in PBS (PBST) for 2 hours at room temperature (RT) followed by incubation with a primary antibody against c-Fos (1:500; Synaptic Systems, Germany), CαMKIIα (1:200; Thermo Fisher Scientific, US), Gad67 (1:500; Merck Millipore, US), and S100β (1:800; Proteintech Group, US) overnight at 4°C. Slices were washed three times with PBST for 10 min each and then incubated with a fluorescent secondary antibody (donkey anti-rabbit Alexa Fluor 488 or 567; 1:500, Molecular Probes, Life Technology, US) for 2 hours at RT. After washing with PBST, the slices were incubated with 4′,6-diamidino-2-phenylindole (DAPI) solution (Beyotime, China) for nuclear labeling and subsequently mounted onto slides with Fluoromount aqueous mounting medium (Sigma-Aldrich, St. Louis, Missouri, US). Images were taken using a confocal laser scanning microscope (Nikon, Japan). The number and fluorescence intensity of c-Fos–positive cells were measured using ImageJ software (National Institutes of Health, US), as we described previously (*46*), in a manner blind to the experimental condition. The vHPC was outlined as a region of interest based on the DAPI staining of the slices.

Western blotting

Tissues were homogenized in a precooled radioimmunoprecipitation assay (Beyotime, China) containing a protease inhibitor cocktail. The protein concentration was determined using a bicinchoninic acid protein assay (Beyotime, China). Proteins (~20 μg) were separated by SDS–polyacrylamide gel electrophoresis. The separated proteins were transferred to the polyvinylidene fluoride membrane (Millipore, US) and blocked using 5% nonfat milk for 2 hours at RT. Then, the membranes were incubated with the following primary antibodies: Kv4.2 (1:1000, Neuromab, US), phospho-Kv4.2 (1:300, Thr^{607}, Santa Cruz, US), phospho-Kv4.2 (1:1000, Ser^{616}, MyBioSource, US), phospho-Kv4.2 (1:1000, Thr^{602}, Bioss, China), Rap1 (1:1000, Cell Signaling Technology, US), and β-actin (1:2000, Abcam, US), overnight at 4°C. The membranes were then washed with 0.1 M tris-buffered saline with Tween 20 buffer and incubated with horseradish peroxidase–conjugated goat anti-rabbit IgG (immunoglobulin G; Proteintech, China) for 1 hour at RT. Immunoreactivity bands were visualized

by an enhanced chemiluminescence kit (Thermo Fisher Scientific, US). The images were captured with a fluorescent spectral imager (Tanon, China). The optical densities of the bands were quantified by ImageJ software.

RBD pull-down assays for Rap1-GTP detection

The GST pull-down assay for Rap1-GTP (activated Rap1) was performed as previously described (*24*). To achieve an adequate protein yield for the GST pull-down assay, hippocampal tissues from two mice were pooled to prepare a single sample. Each sample was lysed using RBD buffer [150 mM NaCl, 50 mM tris-HCl (pH 7.6), 0.5% Triton X-100, 1 mM phenylmethylsulfonyl fluoride, 1 mM Na_3VO_4, 10 mM NaF, leupeptin (2 μg/ml), and aprotinin (2 μg/ml)]. The cell lysate was incubated with glutathione-Sepharose beads conjugated to GST-RalGDS protein for 60 min at 4°C with rotation. After washing for four times, Rap1-GTP was analyzed by Western blotting using a Rap1 antibody.

Fiber photometry

Mice were deeply anesthetized, and a mixture of 0.15 μl of AAVs-*CaMKII*α-Rap1-CA-2A-mCherry-WPRE and 0.15 μl of AAVs-*CaMKII*α-GCaMP6s or AAVs-*CaMKII*α-mCherry virus was unilaterally coinjected into vHPC (AP = −3.42 mm; ML = +3.50 mm; DV = −3.95 mm). Following the viral injection, a 200-μm-diameter optical fiber (Inper Tech, Hangzhou, Zhejiang, China) was implanted into the vHPC (AP = −3.42 mm; ML = +3.50 mm; DV = −3.90 mm). Fiber photometry data were collected using a three-color multichannel optical fiber recording system (RWD Life Science Co., Ltd., R821, China). Briefly, 470- and 410-nm laser beams were first launched into the fluorescence cube and then into the optical fibers; 470- and 410-nm lasers were used for GCaMP6s signal and autofluorescence measurement. The 410-nm channel was used as the control channel and subtracted from the GCaMP6s channel to eliminate any potential interference caused by autofluorescence, bleaching, and motion effects. All the neuronal calcium signals were recorded during the EPMT. Bulk fluorescence signals were generated and analyzed using Multichannel Fiber Photometry software. The fluorescence responses were calculated using the following formula: z-score = $(F_{Signal} - F_{Basal})/STD\ (F_{Basal})$. F_{Basal} represents the average value of F_{Basal} during the baseline time, while STD (F_{Basal}) represents its standard deviation. After recording, mice were transcardially perfused with 4% PFA and subsequently processed to verify viral expression and the placement of optical fibers. Data were included in the analysis only if the viruses and fibers were accurately placed in the correct hemisphere.

Chemogenetic experiments

To investigate whether the increased vCA1 neuronal activity was responsible for CRS- or Rap1 activation–induced anxiety-like behaviors, mice were bilaterally injected with AAV-*CaMKII*α-hM4D(Gi)-2A-eGFP-WPRE or a mixture of AAV-*CaMKII*α-hM4D(Gi)-2A-eGFP-WPRE and AAV-*CaMKII*α-Rap1-CA-2A-mCherry-WPRE into the vHPC, and the cannulae were implanted directly above the vCA1 region. Twenty minutes before behavioral testing, mice received a local infusion of vehicle into the vCA1 and then returned to their home cage. Approximately 4 hours later, the same mice received a local infusion of clozapine-*N*-oxide (2 μg/μl, 1 μl) into the vCA1 (*74*), followed by the second round of behavioral tests conducted 20 min later.

Acute brain slice preparation

Mice were anesthetized using ether and decapitated, and brains were quickly removed and chilled in well-oxygenated (95% O_2 and 5% CO_2) ice-cold artificial cerebrospinal fluid (ACSF) containing 120 mM choline chloride, 2.5 mM KCl, 7 mM $MgSO_4$, 0.5 mM $CaCl_2$, 1.25 mM NaH_2PO_4, 5 mM sodium ascorbate, 3 mM sodium pyruvate, 26 mM $NaHCO_3$, and 25 mM glucose. Coronal brain slices (320 μm) containing vHPC were cut using a vibrating Leica VT1200S microtome and were subsequently transferred to the same incubation solution at 32°C for 15-min recovery. Then, the brain slices were moved to oxygenated ACSF containing 124 mM NaCl, 2.5 mM KCl, 2 mM $MgSO_4$, 2.5 mM $CaCl_2$, 1.25 mM NaH_2PO_4, 22 mM $NaHCO_3$, and 10 mM glucose at RT for at least 30 min.

Electrophysiological recording

Electrophysiological recording was performed as described previously (*75*). A single slice was transferred to the recording chamber and continuously perfused with oxygenated ACSF. The temperature of ACSF in the chamber was maintained at 29 ± 1°C using an automatic temperature controller (TC-324B, Warner Instruments Co., Hamden, US). Recording patch pipettes were made from filamented borosilicate glass capillary tubes (inner diameter, 0.84 mm) by using a horizontal pipette puller (P-97; Sutter Instrument Co., Novato, US). The patch pipettes were filled with pipette solution containing 125 mM K-gluconate, 5 mM KCl, 2 mM $MgCl_2$, 10 mM Hepes, 0.2 mM EGTA, 2 mM ATP-Mg, and 0.1 mM GTP-Na for most of experiments, if not specified.

To record mEPSCs, the membrane potentials were held at −70 mV. Tetrodotoxin (1 μM), CGP52432 (5 μM), and picrotoxin (100 μM) were added to the bath solution. To record miniature inhibitory postsynaptic currents, the patch pipettes were filled with an intracellular solution containing 100 mM CsCl, 30 mM Cs-methanesulfonate, 5 mM NaCl, 1 mM $MgCl_2$, 10 mM Hepes, 0.2 mM EGTA, 2 mM MgATP, and 0.1 mM NaGTP. The membrane potentials were held at −70 mV, and 6-cyano-7-nitroquinoxaline-2,3-dione (CNQX; 20 μM), D,L-2-amino-5-phosphonovaleric acid (20 μM), and tetrodotoxin (1 μM) were added to the bath solution.

To record APs, CNQX (20 μM) and picrotoxin (100 μM) were added to the bath solution. Cells were recorded at current clamp mode, and a series of depolarizing pulses (0 to 250 pA, increasing at a step of 50 pA) was injected. The input resistance and voltage sag ratio were detected by injecting a −50-pA current pulse. The voltage sag ratio was calculated using the following equation: sag ratio = $V_{max}/V_{ss} = (V_{baseline} - V_{min})/(V_{baseline} - V_{steady})$, in which V_{steady} represents the averaged voltage within 50 ms before the end of current injection, $V_{baseline}$ denotes the resting membrane potential, and V_{min} corresponds to the hyperpolarizing current that induced the minimum voltage. The AP threshold was determined at the point where the AP was initiated and exhibited a >10-fold change in the rising rate. The AP amplitude was measured as the voltage difference between the threshold and the peak of the AP. The fAHP was measured as the difference between the peak following an AP spike and the threshold potential.

To record medium and slow AHPs, CNQX (20 μM) and picrotoxin (100 μM) were added to the bath solution. Cells were recorded at the current clamp mode, with a 200-ms, 400-pA current pulse delivered. The medium AHP was measured at the peak of AHP following the current pulse, while the slow AHP was determined by

averaging the voltage in a time window from 280 to 320 ms after the current pulse and subtracting the baseline voltage.

To record TEA-sensitive current, cells were recorded at the voltage clamp mode with a holding potential of −50 mV. A 100-ms voltage pulse from −50 to +45 mV was applied. To block glutamatergic and GABAergic transmission, CNQX (20 μM), picrotoxin (100 μM), and DL-AP5 (50 μM) were added to the perfusion solution. The TEA-sensitive current was isolated by measuring the difference between the traces obtained after the application of TEA (1 mM) and those obtained before its application.

To record transient A-type currents, cells were recorded at the voltage clamp mode with tetrodotoxin (1 μM), Cd^{2+} (300 μM), TEA (20 mM), CNQX (20 μM), and picrotoxin (100 μM) added to the perfusion solution. A series of pulses (400-ms voltage step from −110 to +40 mV) was applied to the cells. A hyperpolarizing prepulse at −110 mV for 100 ms was used to remove A-type K^+ channel inactivation and allow for subsequent maximum activation. The transient channel was inactivated by the same voltage steps preceded by a depolarizing prepulse of −10 mV for 100 ms, leaving the sustained current of the total outward current. The transient current was then isolated by digitally subtracting the sustained current from the total outward current.

Data were digitized at 10 kHz and low-pass filtered at 3 kHz and were obtained by an Axon 700B Amplifier and Digidata 1440A digital-analog convertor (Molecular Devices). Series resistances (R_s) were maintained within the range of 10 to 20 megohms and continuously monitored throughout the duration of the experiments. If R_s changed more than 20% during recording, the data would be excluded. During A-type current recording, the R_s values were corrected by 60 to 80%, and digital leak subtraction was performed online (P/4). Offline data analysis was performed using Origin 8.5 (Microcal Software, Northampton, US).

Biocytin filling and neuronal reconstruction

Biocytin filling was performed using a patch clamp under whole-cell configuration as previously described (*76*). The pipette tip was filled with a biocytin-free medium, followed by backfilling of the pipette with 0.2% biocytin (Life Technologies Corp., Carlsbad, US) dissolved in the pipette solution. Only neurons that maintained a stable membrane potential for at least 20 min were included. After filling, the pipette was slowly withdrawn along the direction of recording until membrane resealing occurred. The slices were then transferred to 4% PFA overnight for postfixing. Subsequently, the slices were incubated with Avidin Alexa Fluor 488 (Life Technologies Corp., Carlsbad, US) conjugated in PBST overnight at 4°C, followed by three rinses in PBST.

The dendrites of individual biocytin-labeled neurons were acquired using a two-photon laser-scanning microscope (Olympus FVMPE-RS, Japan) equipped with a water-immersed objective lens (25×, 1.05 numerical aperture, 2-mm working distance). The reconstruction and determination of dendritic branches were performed using Neurolucida software (MBF Bioscience, Williston, VT). To further reconstruct the dendritic spines, the coronal sections were cryoprotected in 30% sucrose solution and resectioned at a thickness of 70 μm using a frozen microtome. The resectioned slices were then mounted on a glass slide and coverslipped with the Fluoromount Aqueous Mounting Medium (Vector Laboratories Inc., Burlingame, US). Last, high-resolution images were captured using the UPLSAPO 100× oil-immersion lens (Olympus Corp., Japan) (numerical aperture of 1.40). We used a frame size of 1024 by 1024 pixels without zooming, and serial stack images were taken with a step size of 0.3 μm. The dendritic spines were reconstructed using Neurolucida software. Dendrites located at least 20 μm away from the soma and longer than 15 μm were randomly selected for the analysis of spine density. Total dendritic spines and mushroom spines (with a head diameter larger than 0.5 μm and a head-to-neck diameter ratio greater than 1.1) were quantified and classified.

Statistics

Statistical tests were performed using GraphPad Prism (GraphPad Software Inc., US). The normality of the data distribution was confirmed by the Shapiro-Wilk normality test. For unpaired comparison between the two experimental groups, the two-tailed unpaired Student's *t* test (for normally distributed data) or Mann-Whitney *U* test (for nonnormally distributed data) was used. For paired comparison between the two experimental groups, the two-tailed paired *t* test (for normally distributed data) or Wilcoxon matched-pairs signed-rank test (for nonnormally distributed data) was performed. Comparison among three experimental groups was conducted using one-way analysis of variance (ANOVA) followed by Holm-Sidak's post hoc test (for normally distributed data) or Kruskal-Wallis test followed by Dunn's post hoc test (for nonnormally distributed data). For analyzing multiple factors and their interactions, two-way ANOVA or two-way repeated-measures ANOVA followed by a post hoc Sidak's test was used. The statistical significance was considered at $P < 0.05$.

Supplementary Materials

This PDF file includes:

Figs. S1 to S8

REFERENCES AND NOTES

1. GDB 2019 Mental Disorders Collaborators, Global, regional, and national burden of 12 mental disorders in 204 countries and territories, 1990–2019: A systematic analysis for the Global Burden of Disease Study 2019. *Lancet Psychiatry* **9**, 137–150 (2022).
2. D. Arias, S. Saxena, S. Verguet, Quantifying the global burden of mental disorders and their economic value. *eClinicalMedicine* **54**, 101675 (2022).
3. B. W. Penninx, D. S. Pine, E. A. Holmes, A. Reif, Anxiety disorders. *Lancet* **397**, 914–927 (2021).
4. A. Garakani, J. W. Murrough, R. C. Freire, R. P. Thom, K. Larkin, F. D. Buono, D. V. Iosifescu, Pharmacotherapy of anxiety disorders: Current and emerging treatment options. *Front. Psych.* **11**, 595584 (2020).
5. A. Tomar, T. J. McHugh, The impact of stress on the hippocampal spatial code. *Trends Neurosci.* **45**, 120–132 (2022).
6. H.-J. Shi, S. Wang, X.-P. Wang, R.-X. Zhang, L.-J. Zhu, Hippocampus: Molecular, cellular, and circuit features in anxiety. *Neurosci. Bull.* **39**, 1009–1026 (2023).
7. M. S. Fanselow, H.-W. Dong, Are the dorsal and ventral hippocampus functionally distinct structures? *Neuron* **65**, 7–19 (2010).
8. J. J. Knierim, The hippocampus. *Curr. Biol.* **25**, R1116–R1121 (2015).
9. K. G. Kjelstrup, F. A. Tuvnes, H.-A. Steffenach, R. Murison, E. I. Moser, M.-B. Moser, Reduced fear expression after lesions of the ventral hippocampus. *Proc. Natl. Acad. Sci. U.S.A.* **99**, 10825–10830 (2002).
10. M. A. Trivedi, G. D. Coover, Lesions of the ventral hippocampus, but not the dorsal hippocampus, impair conditioned fear expression and inhibitory avoidance on the elevated T-maze. *Neurobiol. Learn. Mem.* **81**, 172–184 (2004).
11. M. A. Kheirbek, L. J. Drew, N. S. Burghardt, D. O. Costantini, L. Tannenholz, S. E. Ahmari, H. Zeng, A. A. Fenton, R. Hen, Differential control of learning and anxiety along the dorsoventral axis of the dentate gyrus. *Neuron* **77**, 955–968 (2013).
12. X. Li, Z.-J. Du, J.-N. Xu, Z.-M. Liang, S. Lin, H. Chen, S.-J. Li, X.-W. Li, J.-M. Yang, T.-M. Gao, mGluR5 in hippocampal CA1 pyramidal neurons mediates stress-induced anxiety-like behavior. *Neuropsychopharmacology* **48**, 1164–1174 (2023).
13. J. C. Schwamborn, A. W. Püschel, The sequential activity of the GTPases Rap1B and Cdc42 determines neuronal polarity. *Nat. Neurosci.* **7**, 923–929 (2004).

14. B. Boettner, L. Van Aelst, Control of cell adhesion dynamics by Rap1 signaling. *Curr. Opin. Cell Biol.* **21**, 684–693 (2009).
15. M. R. Vossler, H. Yao, R. D. York, M.-G. Pan, C. S. Rim, P. J. S. Stork, cAMP activates MAP kinase and Elk-1 through a B-Raf- and Rap1-dependent pathway. *Cell* **89**, 73–82 (1997).
16. R. D. York, H. Yao, T. Dillon, C. L. Ellig, S. P. Eckert, E. W. McCleskey, P. J. S. Stork, Rap1 mediates sustained MAP kinase activation induced by nerve growth factor. *Nature* **392**, 622–626 (1998).
17. A. Jaśkiewicz, B. Pająk, A. Orzechowski, The many faces of Rap1 GTPase. *Int. J. Mol. Sci.* **19**, 2848 (2018).
18. J. J. Zhu, Y. Qin, M. Zhao, L. Van Aelst, R. Malinow, Ras and Rap control AMPA receptor trafficking during synaptic plasticity. *Cell* **110**, 443–455 (2002).
19. S. J. Franco, I. Martinez-Garay, C. Gil-Sanz, S. R. Harkins-Perry, U. Müller, Reelin regulates cadherin function via Dab1/Rap1 to control neuronal migration and lamination in the neocortex. *Neuron* **69**, 482–497 (2011).
20. B. Shah, D. Lutter, Y. Tsytsyura, N. Glyvuk, A. Sakakibara, J. Klingauf, A. W. Püschel, Rap1 GTPases are master regulators of neural cell polarity in the developing neocortex. *Cereb. Cortex* **27**, 1253–1269 (2017).
21. B.-X. Pan, F. Vautier, W. Ito, V. Y. Bolshakov, A. Morozov, Enhanced cortico-amygdala efficacy and suppressed fear in absence of Rap1. *J. Neurosci.* **28**, 2089–2098 (2008).
22. A. Morozov, I. A. Muzzio, R. Bourtchouladze, N. Van-Strien, K. Lapidus, D. Yin, D. G. Winder, J. P. Adams, J. D. Sweatt, E. R. Kandel, Rap1 couples cAMP signaling to a distinct pool of p42/44MAPK regulating excitability, synaptic plasticity, learning, and memory. *Neuron* **39**, 309–325 (2003).
23. T. Nagai, S. Nakamuta, K. Kuroda, S. Nakauchi, T. Nishioka, T. Takano, X. Zhang, D. Tsuboi, Y. Funahashi, T. Nakano, J. Yoshimoto, K. Kobayashi, M. Uchigashima, M. Watanabe, M. Miura, A. Nishi, K. Kobayashi, K. Yamada, M. Amano, K. Kaibuchi, Phosphoproteomics of the dopamine pathway enables discovery of Rap1 activation as a reward signal in vivo. *Neuron* **89**, 550–565 (2016).
24. Z. Zhang, W. Zhang, S. Huang, Q. Sun, Y. Wang, Y. Hu, N. Sun, Y. Zhang, Z. Jiang, N. Minato, J.-P. Pin, L. Su, J. Liu, GABAB receptor promotes its own surface expression by recruiting a Rap1-dependent signaling cascade. *J. Cell Sci.* **128**, 2302–2313 (2015).
25. W.-B. Chen, H.-Q. Pan, Y. He, X.-H. Wang, W.-H. Zhang, B.-X. Pan, Rap1b but not Rap1a in the forebrain is required for learned fear. *Cell Biosci.* **10**, 107 (2020).
26. B. Xu, J. L. Roos, S. Levy, E. J. van Rensburg, J. A. Gogos, M. Karayiorgou, Strong association of de novo copy number mutations with sporadic schizophrenia. *Nat. Genet.* **40**, 880–885 (2008).
27. B. Xu, A. Woodroffe, L. Rodriguez-Murillo, J. L. Roos, E. J. van Rensburg, G. R. Abecasis, J. A. Gogos, M. Karayiorgou, Elucidating the genetic architecture of familial schizophrenia using rare copy number variant and linkage scans. *Proc. Natl. Acad. Sci. U.S.A.* **106**, 16746–16751 (2009).
28. C. M. Middeldorp, J. M. Vink, J. M. Hettema, E. J. C. de Geus, K. S. Kendler, G. Willemsen, M. C. Neale, D. I. Boomsma, X. Chen, An association between Epac-1 gene variants and anxiety and depression in two independent samples. *Am. J. Med. Genet. B Neuropsychiatr. Genet.* **153B**, 214–219 (2010).
29. Y. Dwivedi, A. C. Mondal, H. S. Rizavi, G. Faludi, M. Palkovits, A. Sarosi, R. R. Conley, G. N. Pandey, Differential and brain region–specific regulation of Rap-1 and Epac in depressed suicide victims. *Arch. Gen. Psychiatry* **63**, 639–648 (2006).
30. P. Yuan, R. Zhou, Y. Wang, X. Li, J. Li, G. Chen, X. Guitart, H. K. Manji, Altered levels of extracellular signal-regulated kinase signaling proteins in postmortem frontal cortex of individuals with mood disorders and schizophrenia. *J. Affect. Disord.* **124**, 164–169 (2010).
31. B. A. Kermath, A. M. Vanderplow, K. J. Bjornson, E. N. Seablom, A. M. Novak, C. R. Bernhardt, M. E. Cahill, The Rap1 small GTPase is a critical mediator of the effects of stress on prefrontal cortical dysfunction. *Mol. Psychiatry* **26**, 3223–3239 (2021).
32. N. Tsukamoto, M. Hattori, H. Yang, J. L. Bos, N. Minato, Rap1 GTPase-activating protein SPA-1 negatively regulates cell adhesion. *J. Biol. Chem.* **274**, 18463–18469 (1999).
33. W.-Z. Liu, S.-H. Huang, Y. Wang, C.-Y. Wang, H.-Q. Pan, K. Zhao, P. Hu, B.-X. Pan, W.-H. Zhang, Medial prefrontal cortex input to basolateral amygdala controls acute stress-induced short-term anxiety-like behavior in mice. *Neuropsychopharmacology* **48**, 734–744 (2023).
34. A. J. Apicelli, E. J. Uhlmann, R. L. Baldwin, H. Ding, A. Nagy, A. Guha, D. H. Gutmann, Role of the Rap1 GTPase in astrocyte growth regulation. *Glia* **42**, 225–234 (2003).
35. M. E. Cahill, R. C. Bagot, A. M. Gancarz, D. M. Walker, H. Sun, Z.-J. Wang, E. A. Heller, J. Feng, P. J. Kennedy, J. W. Koo, H. M. Cates, R. L. Neve, L. Shen, D. M. Dietz, E. J. Nestler, Bidirectional synaptic structural plasticity after chronic cocaine administration occurs through Rap1 small GTPase signaling. *Neuron* **89**, 566–582 (2016).
36. S. W. Flavell, M. E. Greenberg, Signaling mechanisms linking neuronal activity to gene expression and plasticity of the nervous system. *Annu. Rev. Neurosci.* **31**, 563–590 (2008).
37. C. Fee, T. Prevot, K. Misquitta, M. Banasr, E. Sibille, Chronic stress-induced behaviors correlate with exacerbated acute stress-induced cingulate cortex and ventral hippocampus activation. *Neuroscience* **440**, 113–129 (2020).
38. J. C. Jimenez, K. Su, A. R. Goldberg, V. M. Luna, J. S. Biane, G. Ordek, P. Zhou, S. K. Ong, M. A. Wright, L. Zweifel, L. Paninski, R. Hen, M. A. Kheirbek, Anxiety cells in a hippocampal-hypothalamic circuit. *Neuron* **97**, 670–683.e6 (2018).
39. G. E. Paquelet, K. Carrion, C. O. Lacefield, P. Zhou, R. Hen, B. R. Miller, Single-cell activity and network properties of dorsal raphe nucleus serotonin neurons during emotionally salient behaviors. *Neuron* **110**, 2664–2679.e8 (2022).
40. B. L. Roth, DREADDs for neuroscientists. *Neuron* **89**, 683–694 (2016).
41. H.-B. Nguyen, R. C. Bagot, J. Diorio, T. P. Wong, M. J. Meaney, Maternal care differentially affects neuronal excitability and synaptic plasticity in the dorsal and ventral hippocampus. *Neuropsychopharmacology* **40**, 1590–1599 (2015).
42. J. Kim, Y. Lei, X.-Y. Lu, C. S. Kim, Glucocorticoid-glucocorticoid receptor-HCN1 channels reduce neuronal excitability in dorsal hippocampal CA1 neurons. *Mol. Psychiatry* **27**, 4035–4049 (2022).
43. T. C. Dumas, T. Gillette, D. Ferguson, K. Hamilton, R. M. Sapolsky, Anti-glucocorticoid gene therapy reverses the impairing effects of elevated corticosterone on spatial memory, hippocampal neuronal excitability, and synaptic plasticity. *J. Neurosci.* **30**, 1712–1720 (2010).
44. M. Mucha, A. E. Skrzypiec, E. Schiavon, B. K. Attwood, E. Kucerova, R. Pawlak, Lipocalin-2 controls neuronal excitability and anxiety by regulating dendritic spine formation and maturation. *Proc. Natl. Acad. Sci. U.S.A.* **108**, 18436–18441 (2011).
45. P. Sah, E. S. Louise Faber, Channels underlying neuronal calcium-activated potassium currents. *Prog. Neurobiol.* **66**, 345–353 (2002).
46. W.-H. Zhang, W.-Z. Liu, Y. He, W.-J. You, J.-Y. Zhang, H. Xu, X.-L. Tian, B.-M. Li, L. Mei, A. Holmes, B.-X. Pan, Chronic stress causes projection-specific adaptation of amygdala neurons via small-conductance calcium-activated potassium channel downregulation. *Biol. Psychiatry* **85**, 812–828 (2019).
47. J.-H. Hu, C. Malloy, G. T. Tabor, J. J. Gutzmann, Y. Liu, D. Abebe, R.-M. Karlsson, S. Durell, H. A. Cameron, D. A. Hoffman, Activity-dependent isomerization of Kv4.2 by Pin1 regulates cognitive flexibility. *Nat. Commun.* **11**, 1567 (2020).
48. B. Juarez, M.-S. Kong, Y. S. Jo, J. E. Elum, J. X. Yee, S. Ng-Evans, M. Cline, A. C. Hunker, M. A. Quinlan, M. A. Baird, A. J. Elerding, M. Johnson, D. Ban, A. Mendez, N. L. Goodwin, M. E. Soden, L. S. Zweifel, Temporal scaling of dopamine neuron firing and dopamine release by distinct ion channels shape behavior. *Sci. Adv.* **9**, eadg8869 (2023).
49. Y. Carrasquillo, J. M. Nerbonne, IA channels: Diverse regulatory mechanisms. *Neuroscientist* **20**, 104–111 (2014).
50. P. Serôdio, B. Rudy, Differential expression of Kv4 K^+ channel subunits mediating subthreshold transient K^+ (A-Type) currents in rat brain. *J. Neurophysiol.* **79**, 1081–1091 (1998).
51. L. A. Schrader, S. G. Birnbaum, B. M. Nadin, Y. Ren, D. Bui, A. E. Anderson, J. D. Sweatt, ERK/MAPK regulates the Kv4.2 potassium channel by direct phosphorylation of the pore-forming subunit. *Am. J. Physiol. Cell Physiol.* **290**, C852–C861 (2006).
52. G. Aceto, C. Colussi, L. Leone, S. Fusco, M. Rinaudo, F. Scala, T. A. Green, F. Laezza, M. D'Ascenzo, C. Grassi, Chronic mild stress alters synaptic plasticity in the nucleus accumbens through GSK3β-dependent modulation of Kv4.2 channels. *Proc. Natl. Acad. Sci. U.S.A.* **117**, 8143–8153 (2020).
53. K. J. Bjornson, A. M. Vanderplow, Y. Yang, D. R. Anderson, B. A. Kermath, M. E. Cahill, Stress-mediated dysregulation of the Rap1 small GTPase impairs hippocampal structure and function. *iScience* **26**, 107566 (2023).
54. Y. Wang, Y. Su, G. Yu, X. Wang, X. Chen, B. Yu, Y. Cheng, R. Li, J. C. Sáez, C. Yi, L. Xiao, J. Niu, Reduced oligodendrocyte precursor cell impairs astrocytic development in early life stress. *Adv. Sci.* **8**, e2101181 (2021).
55. A. Vyas, A. G. Pillai, S. Chattarji, Recovery after chronic stress fails to reverse amygdaloid neuronal hypertrophy and enhanced anxiety-like behavior. *Neuroscience* **128**, 667–673 (2004).
56. Z. Fu, S. H. Lee, A. Simonetta, J. Hansen, M. Sheng, D. T. S. Pak, Differential roles of Rap1 and Rap2 small GTPases in neurite retraction and synapse elimination in hippocampal spiny neurons. *J. Neurochem.* **100**, 118–131 (2007).
57. L. Zhang, P. Zhang, G. Wang, H. Zhang, Y. Zhang, Y. Yu, M. Zhang, J. Xiao, P. Crespo, J. W. Hell, L. Lin, R. L. Huganir, J. J. Zhu, Ras and Rap signal bidirectional synaptic plasticity via distinct subcellular microdomains. *Neuron* **98**, 783–800.e4 (2018).
58. D. M. Bannerman, M. Grubb, R. M. J. Deacon, B. K. Yee, J. Feldon, J. N. P. Rawlins, Ventral hippocampal lesions affect anxiety but not spatial learning. *Behav. Brain Res.* **139**, 197–213 (2003).
59. C.-H. Chang, P.-W. Gean, The ventral hippocampus controls stress-provoked impulsive aggression through the ventromedial hypothalamus in post-weaning social isolation mice. *Cell Rep.* **28**, 1195–1205.e3 (2019).
60. Z. Dong, W. Chen, C. Chen, H. Wang, W. Cui, Z. Tan, H. Robinson, N. Gao, B. Luo, L. Zhang, K. Zhao, W.-C. Xiong, L. Mei, CUL3 deficiency causes social deficits and anxiety-like behaviors by impairing excitation-inhibition balance through the promotion of Cap-dependent translation. *Neuron* **105**, 475–490.e6 (2020).
61. S.-S. Lv, X.-J. Lv, Y.-Q. Cai, X.-Y. Hou, Z.-Z. Zhang, G.-H. Wang, L.-Q. Chen, N. Lv, Y.-Q. Zhang, Corticotropin-releasing hormone neurons control trigeminal neuralgia-induced anxiodepression via a hippocampus-to-prefrontal circuit. *Sci. Adv.* **10**, eadj4196 (2024).
62. J. Hu, C. Malloy, D. A. Hoffman, P38 regulates kainic acid-induced seizure and neuronal firing via Kv4.2 phosphorylation. *Int. J. Mol. Sci.* **21**, 5921 (2020).

63. J. P. Adams, A. E. Anderson, A. W. Varga, K. T. Dineley, R. G. Cook, P. J. Pfaffinger, J. D. Sweatt, The A-type potassium channel Kv4.2 is a substrate for the mitogen-activated protein kinase ERK. *J. Neurochem.* **75**, 2277–2287 (2000).
64. X.-Y. Li, S.-Y. Zhang, Y.-Z. Hong, Z.-G. Chen, Y. Long, D.-H. Yuan, J.-J. Zhao, S.-S. Tang, H. Wang, H. Hong, TGR5-mediated lateral hypothalamus-dCA3-dorsolateral septum circuit regulates depressive-like behavior in male mice. *Neuron* **112**, 1795–1814.e10 (2024).
65. S. G. Birnbaum, A. W. Varga, L.-L. Yuan, A. E. Anderson, J. D. Sweatt, L. A. Schrader, Structure and function of Kv4-family transient potassium channels. *Physiol. Rev.* **84**, 803–833 (2004).
66. L. A. Kim, J. Furst, D. Gutierrez, M. H. Butler, S. Xu, S. A. N. Goldstein, N. Grigorieff, Three-dimensional structure of Ito: Kv4.2-KChIP2 ion channels by electron microscopy at 21 Å resolution. *Neuron* **41**, 513–519 (2004).
67. H. Wang, Y. Yan, Q. Liu, Y. Huang, Y. Shen, L. Chen, Y. Chen, Q. Yang, Q. Hao, K. Wang, J. Chai, Structural basis for modulation of Kv4 K^+ channels by auxiliary KChIP subunits. *Nat. Neurosci.* **10**, 32–39 (2007).
68. Y. Kise, G. Kasuya, H. H. Okamoto, D. Yamanouchi, K. Kobayashi, T. Kusakizako, T. Nishizawa, K. Nakajo, O. Nureki, Structural basis of gating modulation of Kv4 channel complexes. *Nature* **599**, 158–164 (2021).
69. S. Ciocchi, J. Passecker, H. Malagon-Vina, N. Mikus, T. Klausberger, Selective information routing by ventral hippocampal CA1 projection neurons. *Science* **348**, 560–563 (2015).
70. N. Padilla-Coreano, S. S. Bolkan, G. M. Pierce, D. R. Blackman, W. D. Hardin, A. L. Garcia-Garcia, T. J. Spellman, J. A. Gordon, Direct ventral hippocampal-prefrontal input is required for anxiety-related neural activity and behavior. *Neuron* **89**, 857–866 (2016).
71. C. Sánchez-Bellot, R. AlSubaie, K. Mishchanchuk, R. W. S. Wee, A. F. MacAskill, Two opposing hippocampus to prefrontal cortex pathways for the control of approach and avoidance behaviour. *Nat. Commun.* **13**, 339 (2022).
72. G. Pi, D. Gao, D. Wu, Y. Wang, H. Lei, W. Zeng, Y. Gao, H. Yu, R. Xiong, T. Jiang, S. Li, X. Wang, J. Guo, S. Zhang, T. Yin, T. He, D. Ke, R. Li, H. Li, G. Liu, X. Yang, M.-H. Luo, X. Zhang, Y. Yang, J.-Z. Wang, Posterior basolateral amygdala to ventral hippocampal CA1 drives approach behaviour to exert an anxiolytic effect. *Nat. Commun.* **11**, 183 (2020).
73. W.-Z. Liu, W.-H. Zhang, Z.-H. Zheng, J.-X. Zou, X.-X. Liu, S.-H. Huang, W.-J. You, Y. He, J.-Y. Zhang, X.-D. Wang, B.-X. Pan, Identification of a prefrontal cortex-to-amygdala pathway for chronic stress-induced anxiety. *Nat. Commun.* **11**, 2221 (2020).
74. E. C. Cope, S. H. Wang, R. C. Waters, I. R. Gore, B. Vasquez, B. J. Laham, E. Gould, Activation of the CA2-ventral CA1 pathway reverses social discrimination dysfunction in *Shank3B* knockout mice. *Nat. Commun.* **14**, 1750 (2023).
75. H.-Q. Pan, X.-X. Liu, Y. He, J. Zhou, C.-Z. Liao, W.-J. You, S.-Y. Jiang, X. Qin, W.-B. Chen, E.-K. Fei, W.-H. Zhang, B.-X. Pan, Prefrontal GABAA(δ)R promotes fear extinction through enabling the plastic regulation of neuronal intrinsic excitability. *J. Neurosci.* **42**, 5755–5770 (2022).
76. J.-Y. Zhang, T.-H. Liu, Y. He, H.-Q. Pan, W.-H. Zhang, X.-P. Yin, X.-L. Tian, B.-M. Li, X.-D. Wang, A. Holmes, T.-F. Yuan, B.-X. Pan, Chronic stress remodels synapses in an amygdala circuit–specific manner. *Biol. Psychiatry* **85**, 189–201 (2019).

Acknowledgments

Funding: This work was supported by the National Natural Science Foundation of China (grant nos. 32222034 and 81601179 to W.-H.Z.; 82430048, 82125010, and 81930032 to B.-X.P.; 32160193 to H.-Q.P.; 82101589 to W.-Z.L.; and 32100822 to W.-B.C.), the Natural Science Foundation of Jiangxi Province (grant nos. 20242BAB24003 to B.-X.P. and 20242BAB20383 to H.-Q.P.), the Interdisciplinary Innovation Fund Project of Nanchang University (PYJX20230001), and Fund of School of Basic Medical Sciences, Nanchang University. **Author contributions:** Conceptualization: W.-H.Z. Project administration: H.-Q.P., B.-X.P., and W.-H.Z. Investigation: H.-Q.P., W.-Z.L., C.-Z.Y., S.-Y.J., and W.-B.C. Methodology: S.-Y.J., M.-X.Z., H.-T.Y., and Y.-Q.L. Validation: H.-Q.P., C.-Z.Y., S.-Y.J., M.-X.Z., and Y.-Y.W. Formal analysis: H.-Q.P., W.-Z.L., and C.-Z.Y. Resources: H.-Q.P., W.-Z.L., P.H., W.-B.C., L.L., B.-X.P., and W.-H.Z. Data curation: H.-Q.P., C.-Z.Y., and W.-H.Z. Writing—original draft: H.-Q.P., W.-Z.L., B.-X.P., and W.-H.Z. Writing—review and editing: H.-Q.P., J.-L.T., B.-X.P., and W.-H.Z. Visualization: H.-Q.P., W.-Z.L., C.-Z.Y., and W.-H.Z. Supervision: B.-X.P. and W.-H.Z. Funding acquisition: H.-Q.P., W.-Z.L., W.-B.C., B.-X.P., and W.-H.Z. **Competing interests:** The authors declare that they have no competing interests. **Data and materials availability:** All data needed to evaluate the conclusions in the paper are present in the paper and/or the Supplementary Materials.

Submitted 23 September 2024
Accepted 18 April 2025
Published 23 May 2025
10.1126/sciadv.adt3163